strengthened in, T samples (Table 1). These findings are compatible with the "field cancerization" concept in the lung.[29] In our previous study using the Infinium assay, we proved that DNA methylation alterations in N samples resulted in silencing of tumor-related genes in tumorous tissue.[15] However, the correlation between the results of the Infinium assay in N samples and carcinogenetic factors was not examined in detail.

In this epigenetic clustering of patients with LADCs based on DNA methylation profiles in N samples, many of the patients belonging to Cluster I were heavy smokers. In fact, pleural anthracosis, which mainly reflects the long-term cumulative effects of cigarette smoking, was marked in the lungs of patients belonging to Cluster I. Smoking is known to be a cause of COPD. In fact, many patients in Cluster I actually suffered from obstructive ventilation impairment, and histological findings compatible with emphysema and lung fibrosis were observed in their N samples. Moreover, recurrent inflammation is generally associated with COPD,[30] and histological findings compatible with respiratory bronchiolitis[20,21] were actually observed in the lungs of patients belonging to Cluster I. Inflammation is known to be one of the major causes of DNA methylation alterations in precancerous conditions in various organs, such as chronic hepatitis[16,17] and chronic pancreatitis.[31,32] Taken together, the data suggest that the DNA methylation profiles characterizing Cluster I may be established in lung tissue through the long-term cumulative effects of cigarette smoking *via* chronic inflammation under the conditions of COPD. Unlike the previous study, which revealed aberrant DNA methylation of several tumor-related genes in lung cancers themselves of patients with COPD,[33] this study demonstrated for the first time the presence of distinct DNA methylation profiles related to COPD in N samples, based on genome-wide analysis.

The majority of patients belonging to Cluster II were non-smokers, especially young females. DNA methylation profiles characterizing Cluster II may reflect the carcinogenetic pathway that is unrelated to cigarette smoking. Mutation of the *EGFR* gene is well known to be a driver of LADCs in young female non-smokers, especially in Asia.[34] However, Cluster II included LADCs without *EGFR* gene mutations in non-smokers (data not shown), indicating that DNA methylation profiles in Cluster II were not entirely induced by *EGFR* mutation.

Although many of the patients belonging to Cluster III were smokers, the average number of cigarettes smoked per day × year index was lower in Cluster III than in Cluster I. In fact severe pleural anthracosis was not so frequently evident in the lungs of patients belonging to Cluster III. In addition, the incidence of emphysematous change and fibrosis was lower in the adjacent lung tissue of patients in Cluster III than in that of patients in Cluster I. DNA methylation profiles in Cluster III did not develop from a background of chronic inflammation in COPD, but may have developed rapidly before the long-term effects of cigarette smoking had accumulated in the adjacent lung tissue (possibly through more direct effects of carcinogens related or unrelated to cigarette smoking). However, to evaluate more precisely the effects of smoking on DNA methylation profiles, detailed DNA methylation analysis should be performed using purified epithelial cells, such as those from the airway epithelium.

Distinct DNA methylation profiles seem to be established in the non-cancerous lung during the carcinogenetic pathway *via* inflammation in COPD in heavy smokers (Fig. 2*a*), the carcinogenetic pathway unrelated to cigarette smoking (Fig. 2*b*), and the carcinogenetic pathway that occurs not *via* COPD but possibly *via* more direct effects of carcinogens (Fig. 2*c*). Each pathway may have distinct target genes as hallmarks for Clusters I, II and III (Table 3 and Supporting Information Table S3). Among 120 hallmark genes for Clusters I, II and III, 119 (one exception, *ABCC12*, being shared between Clusters II and III) showed ordered differences of DNA methylation from C to N, and then to T samples of the relevant cluster ($p < 0.05$, Jonckheere–Terpstra trend test, Table 3 and Supporting Information Table S3), indicating that a distinct DNA methylation profile in N samples of each cluster is inherited during progression to Ts.

A proportion of genes described in Table 3 and Supporting Information Table S3 may be simple hallmarks of each cluster (simple target genes of each carcinogenetic pathway). However, at least a proportion of DNA methylation alterations occurring during each carcinogenetic pathway actually result in altered expression of target genes, and may participate in establishment of the clinicopathological characteristics of LADCs in each cluster. The DNA methylation profiles in Cluster I may participate in the generation of locally invasive LADCs, which have a large diameter, a progressed T stage, a high histological grade, frequent pleural invasion and tumor anthracosis. DNA methylation profiles in Cluster II may participate in the generation of clinicopathologically less aggressive LADCs with a favorable outcome. DNA methylation profiles in Cluster III may participate in the generation of the most aggressive LADCs showing frequent lymphatic vessel invasion, blood vessel invasion, a high N stage, a high TNM stage and a poor outcome.

Table 3 includes homeobox genes, such as *IRX2* and *HOXD8*, a gene that has been implicated in cell migration, *SPARCL1*, and genes that have been implicated in apoptosis, such as *RGS5* and *EI24*. *IRX2* is known to participate in early lung development in mouse embryos.[35] *HOXD8* is known to be methylated and/or down-regulated in human malignancies, especially in metastatic, rather than in primary lesions.[36,37] *SPARCL1* is an extracellular matrix glycoprotein known to be correlated with cancer invasion.[38,39] *RGS5* is a member of the family of molecules regulating G protein signaling, and stimulates hypoxia-inducible apoptosis.[40] Positive correlations between *RGS5* expression and both tumor differentiation and a favorable outcome have been reported.[41,42] *EI24* is induced by *p53*, suppresses cell growth and induces apoptosis.[43] Reduced expression associated with DNA methylation of *IRX2*, *HOXD8*, *SPARCL1*, *RGS5* and *EI24* in our cohort of LADCs has been confirmed using expression microarray (data not shown). It is

feasible that these target genes of each carcinogenetic pathway participate in determining the clinicopathological characteristics of LADCs in each cluster.

In the validation cohort, the DNA methylation status of hallmark genes identified in N samples of Cluster I was significantly correlated with pleural anthracosis, which reflects the long-term cumulative effects of smoking, and COPD (pulmonary emphysema) in the adjacent lung and tumor anthracosis, which reflect active cancer–stromal interaction in LADCs. The DNA methylation status of the hallmark gene identified in N samples of Cluster II was significantly correlated with lower aggressiveness (low N stage and low TNM stage) of LADCs in the validation cohort. The DNA methylation status of hallmark genes identified in N samples of Cluster III was significantly correlated with aggressiveness of LADCs, such as lymph vessel invasion, a high N stage and a high TNM stage, in the validation cohort. Thus, correlations between distinct DNA methylation profiles in N samples and both carcinogenetic background factors in the adjacent lung tissue and clinicopathological characteristics of LADCs were confirmed in the validation cohort (Table 4).

Receiver operating characteristic curve (ROC) analysis was performed for N samples in the learning cohort, and the thresholds of the representative hallmark genes described in Table 4 were set so that they were nearest to the top left corner of the ROC. Using these thresholds, the sensitivity, specificity and accuracy for prediction of lymphatic vessel involvement, lymph node metastasis, TNM stage and patient outcome (recurrence and death) were calculated in both the learning and validation cohorts (Supporting Information Table S4). Even though Supporting Information Table S4 suggests that the aggressiveness of tumors developing in the same individual patients and patient outcome may be predictable on the basis of DNA methylation status in N samples, further examinations will be needed to set strict criteria for maximal sensitivity, specificity and accuracy.

Although bulk tissue comprising several cell lineages, for a large number of C, N and T samples, was examined in this study, it would be preferable to examine the DNA methylation status of purified cells. Therefore, the DNA methylation status of the representative gene *CASP8* (Infinium probe ID: cg26799474), included in Table 1B, was compared between cancer cells and normal peripheral airway epithelial cells obtained by microdissection from formalin-fixed, paraffin-embedded tissues of representative patients with LADCs and patients without primary lung cancers, respectively, using pyrosequencing. The DNA methylation levels in T samples (0.279 ± 0.184) were significantly lower than those in C samples (0.689 ± 0.042) by Infinium assay ($p = 3.64 \times 10^{-4}$). Such a significant difference was reproduced upon comparison with microdissected normal airway epithelium: pyrosequencing showed that the DNA methylation levels in microdissected cancer cells (0.273 ± 0.313) were significantly lower than those in microdissected normal airway epithelial cells (0.765 ± 0.104) ($p = 2.74 \times 10^{-3}$).

Differences in DNA methylation levels among different cell lineages, such as epithelial and stromal components, are also an important issue. Cancer cells and their stromal cells, such as cancer-associated fibroblasts, were again collected separately by microdissection from formalin-fixed, paraffin-embedded tissues from representative patients with LADCs. The DNA methylation levels of representative genes described in Table 1B were evaluated quantitatively by pyrosequencing. In one of the examined genes (*CASP8* [Infinium probe ID: cg26799474]), the DNA methylation statuses of cancer cells (0.273 ± 0.313) and stromal cells (0.219 ± 0.094) were almost equal, indicating that both may be affected by carcinogenetic factors. For the other examined gene (*LHX1* [Infinium probe ID: cg22660578]), the DNA methylation statuses of cancer cells (0.096 ± 0.141) and stromal cells (0.538 ± 0.486) differed from each other, probably reflecting differences in susceptibility to the effects of carcinogens, or differences in cell lineage.

In summary, DNA methylation profiles reflecting carcinogenetic background factors, such as smoking, inflammation and COPD, appear to be established in adjacent lung tissue in patients with LADCs. Such DNA methylation profiles in adjacent lung tissue may play a role in determining the aggressiveness of tumors developing in the same individual patients, and thus patient outcome.

Acknowledgement

T. Sato is an awardee of a research resident fellowship from the Foundation for Promotion of Cancer Research in Japan.

References

1. Siegel R, Naishadham D, Jemal A. Cancer statistics, 2013. *CA Cancer J Clin* 2013;63:11–30.
2. Sun S, Schiller JH, Gazdar AF. Lung cancer in never smokers—a different disease. *Nat Rev Cancer* 2007;7:778–90.
3. Baylin SB, Jones PA. A decade of exploring the cancer epigenome—biological and translational implications. *Nat Rev Cancer* 2011;11:726–34.
4. Heller G, Zielinski CC, Zochbauer-Muller S. Lung cancer: from single-gene methylation to methylome profiling. *Cancer Metastasis Rev* 2010;29: 95–107.
5. Arai E, Kanai Y. DNA methylation profiles in precancerous tissue and cancers: carcinogenetic risk estimation and prognostication based on DNA methylation status. *Epigenomics* 2010;2: 467–81.
6. Kanai Y. Genome-wide DNA methylation profiles in precancerous conditions and cancers. *Cancer Sci* 2010;101:36–45.
7. Arai E, Chiku S, Mori T, et al. Single-CpG-resolution methylome analysis identifies clinicopathologically aggressive CpG island methylator phenotype clear cell renal cell carcinomas. *Carcinogenesis* 2012;33:1487–93.
8. Zöchbauer-Müller S, Lam S, Toyooka S, et al. Aberrant methylation of multiple genes in the upper aerodigestive tract epithelium of heavy smokers. *Int J Cancer* 2003;107: 612–6.
9. Eguchi K, Kanai Y, Kobayashi K, et al. DNA hypermethylation at the D17S5 locus in non-small cell lung cancers: its association with smoking history. *Cancer Res* 1997;57: 4913–5.
10. Lamy A, Sesboüé R, Bourguignon J, et al. Aberrant methylation of the CDKN2a/p16INK4a gene promoter region in preinvasive bronchial lesions: a prospective study in high-risk patients without invasive cancer. *Int J Cancer* 2002;100: 189–93.
11. Belinsky SA, Palmisano WA, Gilliland FD, et al. Aberrant promoter methylation in bronchial epithelium and sputum from current and former smokers. *Cancer Res* 2002;62:2370–7.

12. Bibikova M, Le J, Barnes B, et al. Genome-wide DNA methylation profiling using Infinium(R) assay. *Epigenomics* 2009;1:177–200.
13. Selamat SA, Chung BS, Girard L, et al. Genome-scale analysis of DNA methylation in lung adenocarcinoma and integration with mRNA expression. *Genome Res* 2012;22:1197–211.
14. Lockwood WW, Wilson IM, Coe BP, et al. Divergent genomic and epigenomic landscapes of lung cancer subtypes underscore the selection of different oncogenic pathways during tumor development. *PLoS One* 2012;7:e37775.
15. Sato T, Arai E, Kohno T, et al. DNA methylation profiles at precancerous stages associated with recurrence of lung adenocarcinoma. *PLoS One* 2013;8:e59444.
16. Nagashio R, Arai E, Ojima H, et al. Carcinogenetic risk estimation based on quantification of DNA methylation levels in liver tissue at the precancerous stage. *Int J Cancer* 2011;129:1170–9.
17. Arai E, Ushijima S, Gotoh M, et al. Genome-wide DNA methylation profiles in liver tissue at the precancerous stage and in hepatocellular carcinoma. *Int J Cancer* 2009;125:2854–62.
18. Ushijima T, Hattori N. Molecular pathways: involvement of Helicobacter pylori-triggered inflammation in the formation of an epigenetic field defect, and its usefulness as cancer risk and exposure markers. *Clin Cancer Res* 2012;18:923–9.
19. Kanai Y, Hirohashi S. Alterations of DNA methylation associated with abnormalities of DNA methyltransferases in human cancers during transition from a precancerous to a malignant state. *Carcinogenesis* 2007;28:2434–42.
20. Garibaldi BT, Illei P, Danoff SK. Bronchiolitis. *Immunol Allergy Clin North Am* 2012;32:601–19.
21. Travis WD, Colby TV, Koss MN, et al. Obstructive pulmonary disease. In: King DW, ed. Atlas of nontumor pathology. Non-neoplastic disorders of the lower respiratory tract. Washington, DC: American Registry of Pathology, 2002:435–71.
22. Kerr KM. Clinical relevance of the new IASLC/ERS/ATS adenocarcinoma classification. *J Clin Pathol* 2013;66:832–8.
23. Noguchi M, Shimosato Y. The development and progression of adenocarcinoma of the lung. *Cancer Treat Res* 1995;72:131–42.
24. Colby TV, Noguchi M, Henschke C, et al. Adenocarcinoma. In: Travis WD, Brambilla E, Muller-Hermelink HK, Harris CC, eds. World health classification of tumours pathology and genetics of tumours of the lung, pleura, thymus and heart. Lyon: IARC Press, 2004:35–44.
25. Wang D, Minami Y, Shu Y, et al. The implication of background anthracosis in the development and progression of pulmonary adenocarcinoma. *Cancer Sci* 2003;94:707–11.
26. Noguchi M, Morikawa A, Kawasaki M, et al. Small adenocarcinoma of the lung. Histologic characteristics and prognosis. *Cancer* 1995;75:2844–52.
27. UICC International Union Against Cancer. Lung and pleural tumours. In: Sobin LH, Gospodarowicz MK, Wittekind C, eds. TNM classification of malignant tumours, 7th edn. Oxford: Wiley-Blackwell, 2009:138–46.
28. Hu L, Sekine M, Gaina A, et al. Association of smoking behavior and socio-demographic factors, work, lifestyle and mental health of Japanese civil servants. *J Occup Health* 2007;49:443–52.
29. Kadara H, Kabbout M, Wistuba II. Pulmonary adenocarcinoma: a renewed entity in 2011. *Respirology* 2012;17:50–65.
30. Decramer M, Janssens W, Miravitlles M. Chronic obstructive pulmonary disease. *Lancet* 2012;379:1341–51.
31. Peng DF, Kanai Y, Sawada M, et al. DNA methylation of multiple tumor-related genes in association with overexpression of DNA methyltransferase 1 (DNMT1) during multistage carcinogenesis of the pancreas. *Carcinogenesis* 2006;27:1160–8.
32. Peng DF, Kanai Y, Sawada M, et al. Increased DNA methyltransferase 1 (DNMT1) protein expression in precancerous conditions and ductal carcinomas of the pancreas. *Cancer Sci* 2005;96:403–8.
33. Suzuki M, Wada H, Yoshino M, et al. Molecular characterization of chronic obstructive pulmonary disease-related non-small cell lung cancer through aberrant methylation and alterations of EGFR signaling. *Ann Surg Oncol* 2010;17:878–88.
34. Sharma SV, Bell DW, Settleman J, et al. Epidermal growth factor receptor mutations in lung cancer. *Nat Rev Cancer* 2007;7:169–81.
35. Mummenhoff J, Houweling AC, Peters T, et al. Expression of Irx6 during mouse morphogenesis. *Mech Dev* 2001;103:193–5.
36. Leshchenko VV, Kuo PY, Shaknovich R, et al. Genomewide DNA methylation analysis reveals novel targets for drug development in mantle cell lymphoma. *Blood* 2010;116:1025–34.
37. Kanai M, Hamada J, Takada M, et al. Aberrant expressions of HOX genes in colorectal and hepatocellular carcinomas. *Oncol Rep* 2010;23:843–51.
38. Hurley PJ, Marchionni L, Simons BW, et al. Secreted protein, acidic and rich in cysteine-like 1 (SPARCL1) is down regulated in aggressive prostate cancers and is prognostic for poor clinical outcome. *Proc Natl Acad Sci USA* 2012;109:14977–82.
39. Turtoi A, Musmeci D, Naccarato AG, et al. Sparc-like protein 1 is a new marker of human glioma progression. *J Proteome Res* 2012;11:5011–21.
40. Jin Y, An X, Ye Z, et al. RGS5, a hypoxia-inducible apoptotic stimulator in endothelial cells. *J Biol Chem* 2009;284:23436–43.
41. Huang G, Song H, Wang R, et al. The relationship between RGS5 expression and cancer differentiation and metastasis in non-small cell lung cancer. *J Surg Oncol* 2012;105:420–4.
42. Wang JH, Huang WS, Hu CR, et al. Relationship between RGS5 expression and differentiation and angiogenesis of gastric carcinoma. *World J Gastroenterol* 2010;16:5642–6.
43. Zhao X, Ayer RE, Davis SL, et al. Apoptosis factor E124/PIG8 is a novel endoplasmic reticulum-localized Bcl-2-binding protein which is associated with suppression of breast cancer invasiveness. *Cancer Res* 2005;65:2125–9.

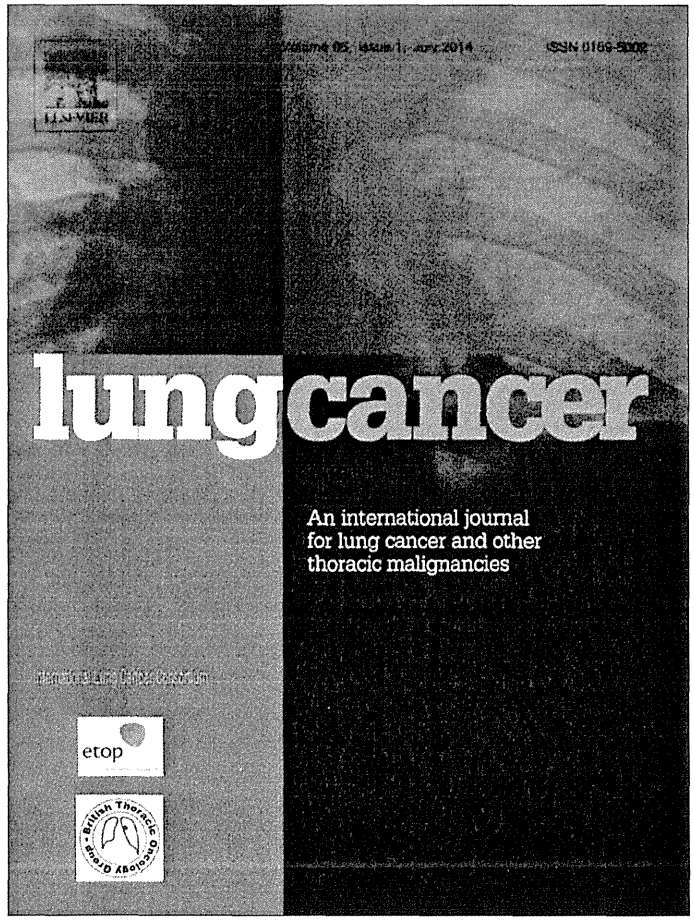

Lung Cancer 85 (2014) 40–46

Contents lists available at ScienceDirect

Lung Cancer

journal homepage: www.elsevier.com/locate/lungcan

Comparison between CT tumor size and pathological tumor size in frozen section examinations of lung adenocarcinoma

Tetsuya Isaka[a,b,c,*], Tomoyuki Yokose[a], Hiroyuki Ito[b], Naoko Imamura[b], Masato Watanabe[b], Kentaro Imai[b], Teppei Nishii[b], Tetsukan Woo[c], Kouzo Yamada[d], Haruhiko Nakayama[b], Munetaka Masuda[c]

[a] Department of Pathology, Kanagawa Cancer Center, 2-3-2 Nakao, Asahi, Yokohama, Kanagawa 241-0815, Japan
[b] Department of Thoracic Surgery, Kanagawa Cancer Center, 2-3-2 Nakao, Asahi, Yokohama, Kanagawa 241-0815, Japan
[c] Department of Surgery, Yokohama City University, 3-9 Fukuura, Kanazawa, Yokohama, Kanagawa 236-0004, Japan
[d] Department of Thoracic Oncology, Kanagawa Cancer Center, 2-3-2 Nakao, Asahi, Yokohama, Kanagawa 241-0815, Japan

ARTICLE INFO

Article history:
Received 30 December 2013
Received in revised form 18 March 2014
Accepted 24 March 2014

Keywords:
Lung cancer
Adenocarcinoma
Inflation method
Pathological tumor size
Frozen section examinations
CT tumor size
Lepidic

ABSTRACT

Objective: We examined the appropriate measurement for pathological tumor size by comparing radiological and pathological tumor size of resected lung adenocarcinoma in FSE.
Materials and methods: We reviewed records of 59 resected specimens of lung adenocarcinoma for FSE from January to December 2008. Specimens were well-inflated with saline by using an injector before cutting into segments. After selecting the tumor segment of maximal diameter, we compared three ways of measuring pathological tumor size by using paired *t*-test: (I) macroscopic tumor size (MTS), measured with a metal straight ruler, (II) microscopic frozen section tumor size (FSTS), and (III) microscopic paraffin section tumor size (PSTS). We compared each discrepancy rate (DR) [DR = (CT tumor size – pathological tumor size)/CT tumor size × 100] (%) between tumors that were air-containing type and solid-density type on CT scans, and also compared the tumors with lepidic component rates (LCR) ≥50% and LCR <50%, by using Mann–Whitney *U*-tests.
Results: FSE could diagnose malignancy with 100% accuracy. The mean CT tumor size was 18.36 mm, and the mean pathological tumor sizes (MTS, FSTS, and PSTS) were 17.81, 14.29, and 14.23 mm, respectively. FSTS and PSTS were significantly smaller than CT tumor size ($p < 0.001$). The DR calculated with PSTS was significantly larger in air-containing than in solid-density tumors, and also larger in LCR ≥50% than in LCR <50% tumors.
Conclusion: FSE with the inflation method diagnosed malignancy with 100% accuracy. The lung specimen must be sufficiently inflated to prevent tissue shrinking, and we propose MTS as the definition for pathological tumor size in FSE. The greater discordance observed between CT tumor size and microscopic tumor size was assumed to be due to shrinkage of the lepidic component in the tumor.

1. Introduction

Recent remarkable developments in diagnostic radiological imaging have allowed more frequent, easier detection of small tumorous lesions. As a result, we more frequently encounter tumors that are difficult to diagnose pre-operatively, which requires us to perform intra-operative frozen section examination (FSE) [1]. FSE is performed to confirm the presence of a tumor inside the resected specimen, to determine if the tumor is benign or malignant, to confirm that the tumor has a sufficient tumor margin, to decide the operation methodology, and to decide the exact stage [1–3]. FSE is a well-established method for definitive diagnosis, and there are few false negatives and positives when FSE is used for small-sized lung cancer [3–5].

However, deflated lung specimen results in the collapse of parenchymal tissue and distortion of lung structures, and pathologists have difficulty with differentiating minute invasive focus from

* Corresponding author at: 1-39-8-307, Futamatagawa, Asahi, Yokohama, Kanagawa 241-0821, Japan. Tel.: +81 45 520 2222; fax: +81 45 520 2202.
E-mail addresses: l401092k@yahoo.co.jp (T. Isaka), yokose-t@kcch.jp (T. Yokose), h-ito@kcch.jp (H. Ito), nao.imamura@kcch.jp (N. Imamura), mit_lan_evo_2@hotmail.co.jp (M. Watanabe), kentaro-imai@tea.ocn.ne.jp (K. Imai), nteppei@par.odn.ne.jp (T. Nishii), tetsu.n.u@cotton.ocn.ne.jp (T. Woo), kozoyama@eb.mbn.or.jp (K. Yamada), nakayama-h@kcch.jp (H. Nakayama), mmasuda@yokohama-cu.ac.jp (M. Masuda).

http://dx.doi.org/10.1016/j.lungcan.2014.03.023
0169-5002/

collapse of small-sized lung adenocarcinoma. Inflation method is known to preserve the morphology of the lung specimen with high diagnostic accuracy of small-sized lung adenocarcinoma in the FSE [6]. Although FSE with inflation method plays an important role in lung adenocarcinoma operations, there are no clear methods or standards established for the preparation of resected specimens, and the technique differs by institution. Some important factors that may differ in FSE preparation include whether or not an inflation method is applied, how the lung specimen is inflated, how the embedding medium is used, and the width of the tissue segment the pathologist cuts [6–8]. There is also no standard method for measurement of characteristics such as pathological tumor size and resected tumor margin of lung specimens in FSE, and these methods differ by institution.

Although Travis et al. previously noted the possibility that estimates of tumor size for tumors that are predominately lepidic were smaller than the actual tumor size of lung adenocarcinoma [9], to our knowledge, there have not been any studies that have examined precisely how much smaller the estimates are. In this study, we determined the appropriate measurement of pathological tumor size by comparing radiological and pathological tumor measurements of resected adenocarcinoma of the lung in FSE using inflation method. Moreover, we evaluated the impact of lepidic component on pathological tumor size.

2. Materials and methods

2.1. Patients

We retrospectively reviewed the records of 59 resected lung specimens from 58 patients for frozen section diagnoses (54 wedges and 5 segmentectomies) of lung adenocarcinoma from Kanagawa Cancer Center Hospital from January to December 2008. Cases in which tumors were positive at the cut-end were excluded. All patients provided informed consent, and the studies were performed according to the requirements of the institutional review board of Kanagawa Cancer Center.

2.2. Preparation procedures for FSE

Our preparation procedures for FSE are shown in Fig. 1. Lung specimens were well-inflated by injection of saline from the cut-end by using an 18-gauge injection needle (Fig. 1a). In order to prevent immediate saline leakage from the lung, the needle was inserted toward the subpleura and turned in some other directions inside the lung specimen so as to minimalize the number of puncture sites. Then, the pathologist (T.Y.) cut the specimen into segments 3–5 mm in width by drawing long cutting knife lightly, not pressingly (Fig. 1b) and immersed the segments in saline for a few minutes (Fig. 1c and d). We selected one or two tissue segments in which the tumor size was considered maximal, and where the tumor growth area was considered to be most predominately non-lepidic. The tumor tissue was put into a 50 mL injector which contained 10–20 mL of 50% embedding medium (Tissue-Tek O.C.T. Compound, Sakura Finetek-USA, CA), and was inflated with negative pressure (Fig. 1e and f). The tissue segment was frozen using dry ice and acetone, then a 2–4 μm cryostat section was made with a Leica CM 1900 UV Cryostat (Leica Microsystems, Wetzlar, Germany) for FSE. After FSE was complete, the tissue sections were melted at room temperature and fixed with 10% neutral buffered formalin to make permanent paraffin sections.

2.3. Measurement of pathological tumor size and CT tumor size

Pathological tumor size was measured in three ways: (I) macroscopic tumor size (MTS) measured by using a metal straight ruler, (II) microscopic tumor size measured on the frozen section (frozen section tumor size, FSTS), and (III) microscopic tumor size measured on the permanent paraffin section (paraffin section tumor size, PSTS). After the specimen was cut into segments and immersed in saline, MTS was measured where the tumor seemed to be maximal in size macroscopically. FSTS and PSTS were measured by performing stereoscopic microscopy and Leica Application Suite image analysis software (Leica Microsystems, Tokyo, Japan) (Fig. 1g and h). Chest CT images were obtained using a X-Vigor/Real CT scanner or an Aquillion CT scanner (Toshiba Medical Systems, Tochigi, Japan), and the CT tumor size was determined from high-resolution CT scans with 1–2 mm section thickness by measuring the maximum axial tumor diameter in a pulmonary window level setting (TSPW; level, −600 HU; width, 1600 HU). We also measured tumor size in a mediastinal window level setting (TSMW: level, 40 HU; width, 400 HU) on high-resolution CT scans.

2.4. Word definitions

We defined tumor shadow disappearance rate (TDR) using the following formula: TDR = [1 − (TSMW/TSPW)] × 100 (%). Tumors with TDR ≥50% and TDR <50% were considered "air-containing types" and "solid-density types", respectively [10,11].

We also calculated discrepancy rate (DR) with the formula: DR = (CT tumor size − each pathological tumor size)/CT tumor size × 100 (%).

We defined the term "lepidic component rate (LCR)" as the area proportion of replacement growth pattern divided by the entire tumor on a permanent paraffin section.

2.5. Statistical analysis

The average CT tumor size and each pathological tumor size were compared by using paired *t*-tests. *T* factor migration according to the Union for International Cancer Control (UICC) guidelines, 7th edition, was assessed by using the likelihood ratio. The correlation between CT tumor size and each pathological tumor size was evaluated by using Pearson's correlation analysis. We compared DR values, which were calculated for each pathological tumor measurement and compared between air-containing type ($n = 44$) and solid-density type ($n = 15$) by using Mann–Whitney *U*-tests. Furthermore, we compared DR values between LCR ≥50% tumors ($n = 40$) and LCR <50% tumors ($n = 19$) by using Mann–Whitney *U*-tests. *p*-values less than 0.05 were considered significant.

3. Results

The clinicopathological characteristics are shown in Table 1. Of the 59 lung specimens for FSE, 28 (47.4%) were adenocarcinoma in situ (AIS), 4 (6.8%) were minimally invasive adenocarcinoma, and 27 (45.8%) were invasive adenocarcinoma. The accuracy of diagnosis of malignancy from frozen sections, based on the final diagnosis made based on the permanent paraffin section, was 100%. Air space in the tumor tissue was dilated enough to differentiate lepidic component from collapse and fibrous foci on frozen section (Fig. 2). Clinical *T* factors (cT1a, cT1b, and cT2a) were 42, 16, and 1, respectively, and the average CT tumor size ±SD was 18.36 ± 5.23 mm (range, 7–33 mm) (Fig. 3). The mean pathological tumor sizes ±SD of MTS, FSTS, PSTS were 17.81 ± 6.32 mm (range, 6–40 mm), 14.29 ± 3.66 mm (range, 5.46–21.21 mm), and 14.23 ± 4.38 mm (range, 5.17–22.92 mm), respectively. The average values for FSTS and PSTS were significantly smaller than the CT-based measurements ($p < 0.001$ for both). In regard to *T* factor migration, there were 8 (13.6%), 14 (23.7%), and 12 (22.0%) cases of down-migration when MTS, FSTS, and PSTS were used, respectively, to measure pathological tumor size, although there were

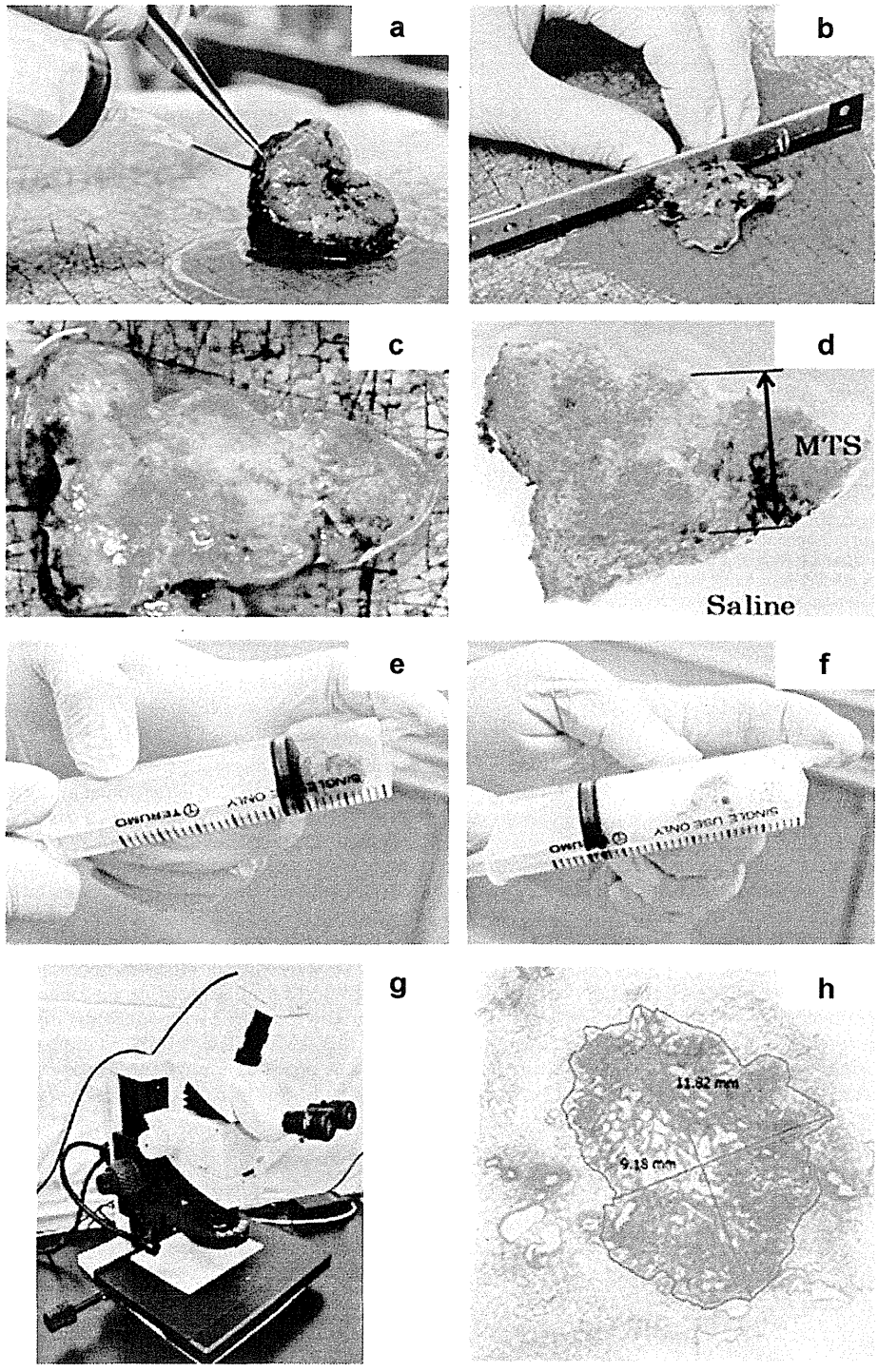

Fig. 1. Procedure for preparation of specimens for FSE. (g and h) FSTS and PSTS were measured with the Leica Application Suite stereoscopic microscope (Leica Microsystems; Tokyo, Japan). After plotting a tumor border region on frozen sections and paraffin sections, the maximum diameter in the area was measured to determine the FSTS and PSTS, respectively.

no cases of up-migration in FSTS and PSTS ($p = 0.0024$) (Fig. 3). Fig. 4 shows the correlation diagrams between CT tumor size and each pathological tumor size. According to the Pearson's correlation analysis, there were significant correlations between CT tumor size and each pathological tumor size (correlation coefficients (r) were 0.766, 0.700, and 0.682, respectively, and all were $p < 0.001$).

Fig. 5 shows the comparison of DR values between air-containing type tumors and solid-density type tumors. DR values calculated with PSTS were significantly larger in air-containing type than solid-density type specimens (27.3% versus 15.5%, $p = 0.032$). Fig. 6 shows the comparison of DR values between LCR ≥50% tumors and LCR <50% tumors. DR values calculated with

Table 1
Characteristics of the 58 patients in the study.

Fifty-eight patients with 59 specimens	
Median age (years)	67 (38–84)
Sex (male:female)	23:35
Side (right:left)	38:20
Lobe (upper:middle:lower)	39:0:20
Operative procedure for rapid diagnosis (partial resection:segmentectomy)	49:10
Pathological classification of adenocarcinoma (%)	
AIS	28 (47.4)
MIA	4 (6.8)
IA	27 (45.8)
(IA-LP:IA-AP:IA-PP:IA-SP:IA-variant)	(10:9:5:2:1)
Mean CT tumor size (mm)	18.36 (7–33)
Clinical *T* factor (%)[a]	
T1a	42 (71.2)
T1b	16 (27.1)
T2a	1 (1.7)
The accuracy of diagnosis of malignancy from frozen sections, based on the final diagnosis made based on the permanent paraffin section (%)	100

AIS, adenocarcinoma in situ; MIA, minimally invasive adenocarcinoma; IA, invasive adenocarcinoma; IA-LP, invasive adenocarcinoma lepidic predominant; IA-AP, invasive adenocarcinoma acinar predominant; IA-PP, invasive adenocarcinoma papillary predominant; IA-SP, invasive adenocarcinoma solid predominant.
[a] UICC 7th edition.

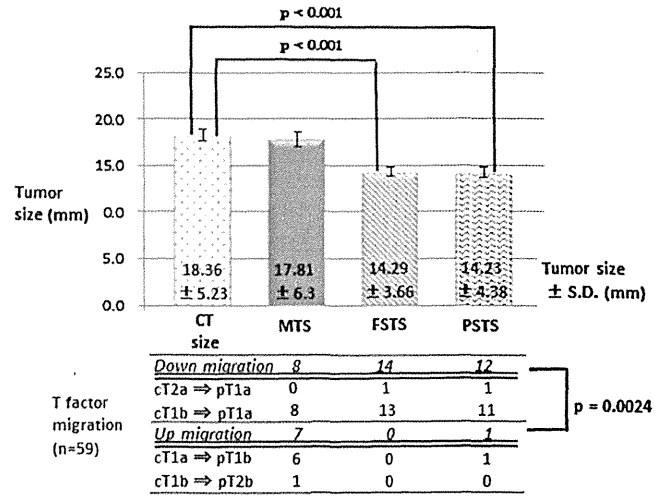

Fig. 3. Tumor size based on CT measurement and various pathological measurement techniques. The average CT tumor size ±SD was 18.36 ± 5.23 mm and the mean pathological tumor sizes ±SD of MTS, FSTS, PSTS were 17.81 ± 6.32 mm, 14.29 ± 3.66 mm, and 14.23 ± 4.38 mm, respectively. The average values for FSTS and PSTS were significantly smaller than the CT-based measurements ($p < 0.001$ for both). In regard to *T* factor migration, there were 8 (13.6%), 14 (23.7%), and 12 (22.0%) cases of down-migration when MTS, FSTS, and PSTS were used, respectively, to measure pathological tumor size, although there were no cases of up-migration in FSTS and PSTS ($p = 0.0024$).

PSTS were significantly larger in LCR ≥50% tumors than LCR <50% tumors (27.0% versus 18.6%, $p = 0.021$).

4. Discussion

4.1. Preparation methodology for FSE

It is considered that our simple inflation method, which includes injection of saline into the resected specimen and immersing the cut segment in saline, makes ambiguous and small-sized tumors more apparent in the gross specimen (Fig. 1c and d). This allows identification of all tumors, including impalpable ones, in FSE specimens. Borczuk et al. previously noted that neoplastic lesions became more apparent over time, and the lesion was often more clearly revealed upon re-examination of the gross specimen after several minutes because of drainage of excess blood and inflation of the lung by the infiltration of saline into the specimen [12]. Another inflation procedure was previously introduced that expands lung tissue by injecting diluted embedding medium into the lung, and this procedure enabled detection of minute and even non-palpable ground-glass opacity lesions much easier in FSE with a high level of diagnostic accuracy [8]. However, embedding medium is more expensive than saline and it costs even more if the lung specimen for frozen section is larger. By contrast, saline is less expensive and is easily obtainable. It is also considered that drainage excess blood by saline is necessary for the visualization and the exact measurement of MTS. Further study is necessary to examine how much effect injection of embedding medium has on each pathological tumor size compared with our saline injection method.

In this study, FSE was 100% accurate for the diagnosis of malignancy. A previous multi-center study noted that the diagnostic accuracy of FSE in thoracic surgery was 98.58% [5]. Marchevsky

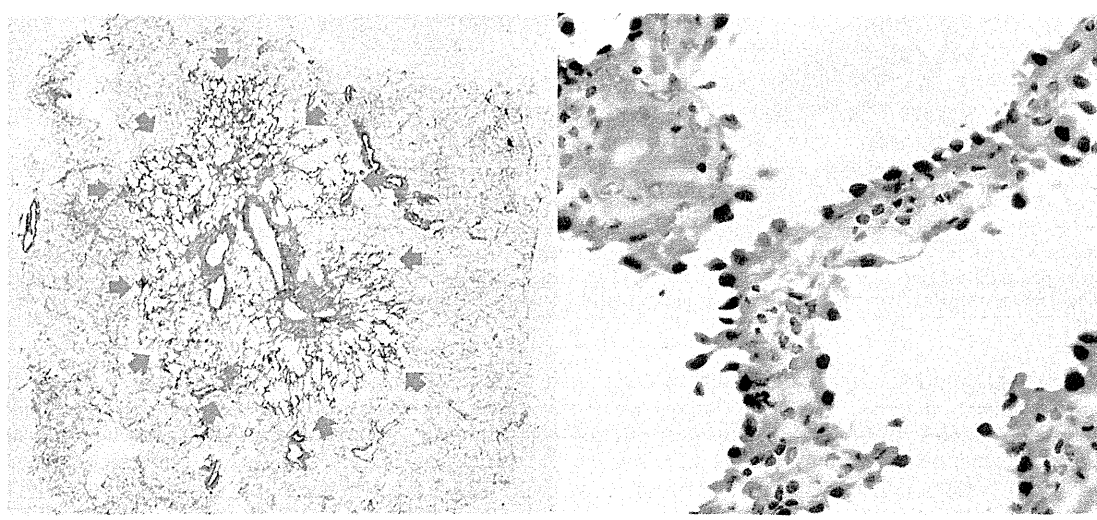

Fig. 2. The figure shows the gross appearance (left) and microscopic feature (right) in a frozen section diagnosed as adenocarcinoma in situ. Air space in the tumor was dilated enough to differentiate lepidic component from collapse and fibrous foci. Accordingly, a small adenocarcinoma in situ lesion was diagnosed readily by frozen section.

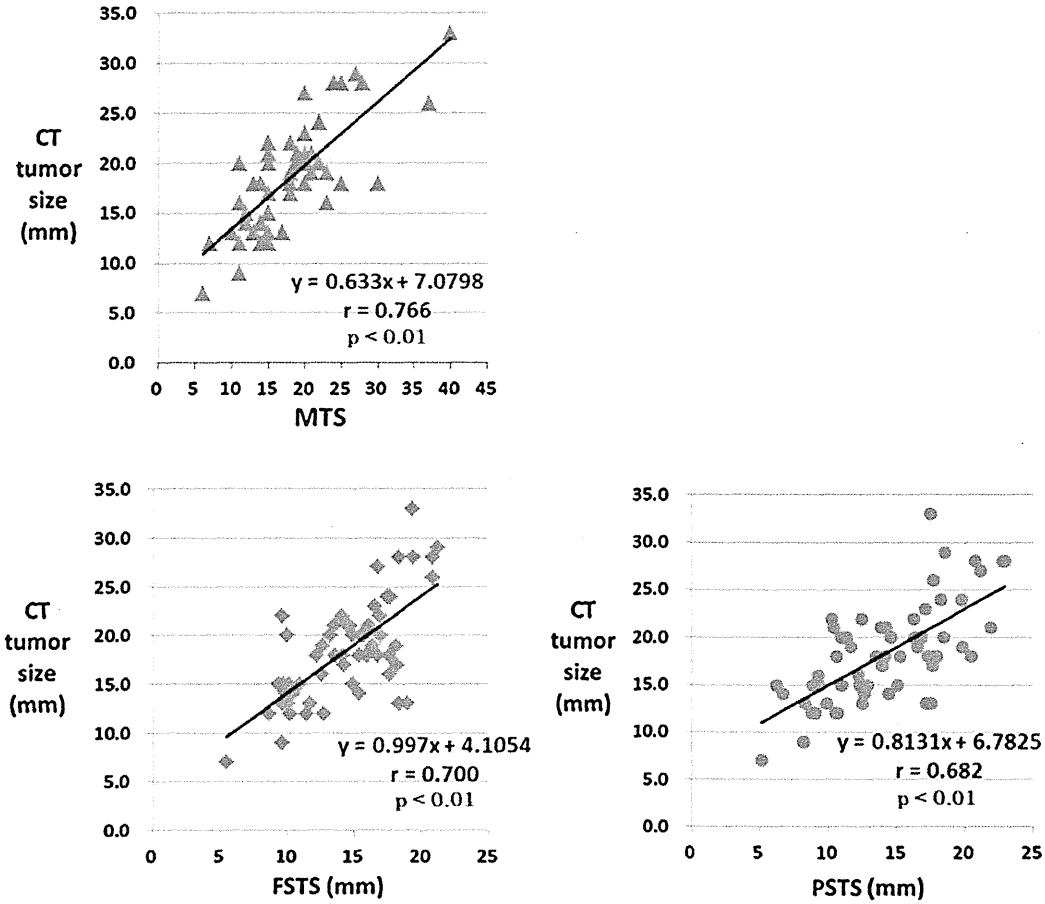

Fig. 4. Diagrams of the correlation between CT tumor size and the size indicated by each pathological measurement. According to the Pearson's correlation analysis, there were significant correlations between CT tumor size and each pathological tumor size (correlation coefficients (r) were 0.766, 0.700, and 0.682, respectively, and all were $p < 0.001$).

et al. also reported that the sensitivity for diagnosis of neoplasia was 86.9% for nodules smaller than 1.1 cm in diameter, and 94.1% for nodules 1.1–1.5 cm [1]. However, the preparation procedures for lung specimens in FSE were not described in these reports. Walts et al. reported that there were 12.1% (27 of 224) of frozen section errors and 6.3% (14 of 224) of deferrals without inflating lung specimens for FSE, and noted that errors and deferrals were more prominent in cases of AIS or minimally invasive adenocarcinoma (MIA), which are 10 mm or less in size [2]. Xu et al. reported that the accuracy was 100% after using the inflation method in FSE, although there were two false-positive cases before using the inflation method. The inflation method facilitated proper evaluation of the morphological alterations in the frozen section, and it made it easier to cut the lung specimen into segments, which reduced the chance of compression during sectioning [6]. With regard to our inflation method, it was possible to identify and diagnose minute precancerous and cancerous foci such as AAH and AIS readily on FSE

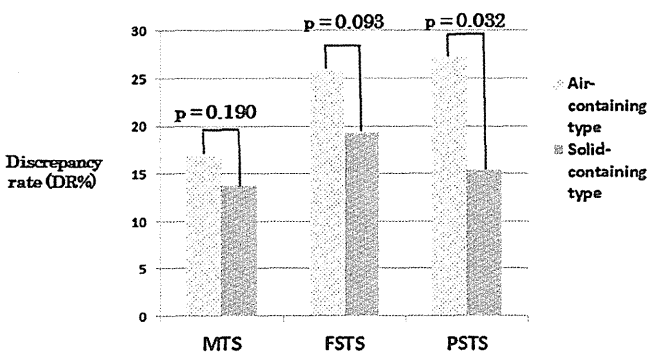

Fig. 5. Comparison of DR values between air-containing type tumors and solid-density type tumors. DR values calculated with PSTS were significantly larger in air-containing type than solid-density type specimens (27.3% versus 15.5%, $p = 0.032$).

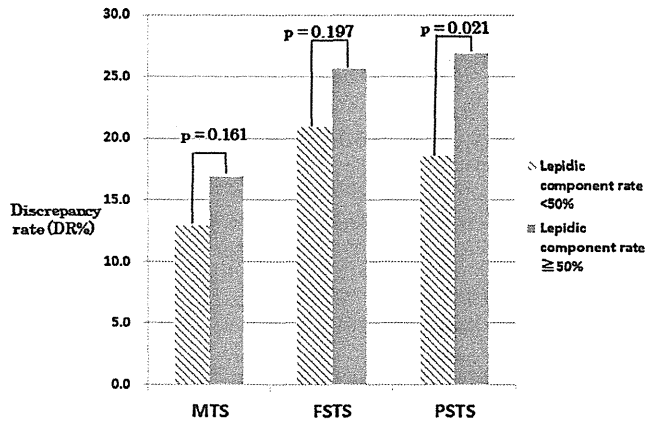

Fig. 6. Comparison of DR values between LCR ≥50% tumors and LCR <50% tumors. DR values calculated with PSTS were significantly larger in LCR ≥50% tumors than LCR <50% tumors (27.0% versus 18.6%, $p = 0.021$).

both macroscopically and microscopically (Fig. 2). In this study, all of 28 AIS lesions were detectable and diagnosed accurately on FSE by using this method (Table 1).

There is no standard method of preparation for resected specimens in FSE, and the methodology differs by institution. Moreover, the definition of pathological tumor size differs among institutions in FSE. In this study, we demonstrated that pathological tumor sizes were markedly different among MTS, PSTS, or FSTS, and clarified the necessity of unifying the pathological tumor size in FSE.

4.2. Comparison between CT tumor size and each pathological tumor size

Since there was a strong correlation between CT tumor size and each pathological tumor size (Fig. 4), and a high accuracy rate for the diagnosis of malignancy, our method of specimen preparation for FSE was considered appropriate to obtain sufficient information about the lung tumor. Among the three pathological measurement methods of tumor size, MTS correlated the best with the CT tumor size ($r = 0.766$) and its mean size was about the same as the CT tumor size (Figs. 3 and 4). Generally, in order to measure a resected margin, we cut lung specimens vertically against the resected surface. We did consider that most of the resection directions were not identical to the axial direction of the CT, but our results indicate that even if the direction varied widely, there was no significant difference between MTS and CT tumor size among the small lung adenocarcinomas.

On the other hand, the average FSTS and PSTS were significantly smaller than the CT tumor size, and caused down-migration of *T* factor (Fig. 3). As a result, we propose that the pathological tumor size for *T* factor should be defined as the MTS in small lung adenocarcinoma in FSE, and FSTS and PSTS should not be used, since patients might lose their chance to receive adjuvant chemotherapy because of the underestimation of their tumor size.

According to the TDR, the small lung adenocarcinomas (20 mm or less) were categorized as air-containing type and solid-density type, with the air-containing type having no evidence of metastasis (pleural involvement, vascular invasion, lymphatic permeation, or lymph node metastasis) and a much better prognosis than the solid-density type [10,11]. In air-containing type tumors, there is evidence of collapse, or collapse with bronchioloalveolar carcinoma, which represents a non-invasive tumor [11]. As shown in Fig. 5, DR values calculated with PSTS were significantly higher in air-containing type than solid-density type tumors ($p = 0.032$). This indicates that, if a tumor classified as air-containing type was pathologically measured using PSTS, the pathological tumor size might be underestimated by as much as 75% of the CT tumor size.

4.3. Interpretation of the discordance between PSTS and CT tumor size

Lampen-Sachar et al. used formalin fixed specimens to show that the mean CT tumor size was statistically larger than the pathological tumor size ($p < 0.001$), and concluded that CT overestimates the tumor size. The author stated that the discordance was due to differences in lung aeration and expansion, and due to the measurement of infiltration and/or edema surrounding the tumor in CT scans [13]. This result was similar to our examination in FSE. However, inflammation, fibrosis, and edema surrounding the tumor are rarely seen in the cases of peripheral small-sized adenocarcinoma which are considered to be an indication for FSE, and especially rare if the tumors were lepidic component predominant. Therefore, MTS was considered to reflect the area of adenocarcinoma accurately. It is considered that the underestimation of pathological tumor size measured with FSTS and PSTS is due to the deep cryosection of the tumor at its maximum diameter, tissue shrinkage by desiccation, and contraction that results from stuffing the tissue into a cassette.

Previously, Travis et al. noted a possibility that estimates of tumor size of lepidic predominant adenocarcinoma were smaller than the actual tumor size [9]. On the basis of this observation, we hypothesized that the lepidic component of the tumor was responsible for the contractility. As shown in Fig. 6, we found that tumors with LCR $\geq$50% were underestimated, giving values about 75% of the CT tumor size, if they were measured by PSTS. This agrees with the results of Fig. 5 pathologically. The reason for the contractility of the lepidic component is unknown, but we hypothesize that tumors which have abundant air space shrink more easily during preparation because of issues such as desiccation, stuffing pressure, and degeneration by the chemical solution, which are part of the preparation process for FSE. Another hypothesis is that inherent elasticity of alveoli which may cause contraction of the tissue is less affected by lepidic morphology as compared to invasive tumor.

4.4. Future tasks in the measurement of pathological tumor size

We propose the use of MTS, which approximated CT tumor size, as the pathological tumor measurement in FSE, although it may become burdensome for pathologists to measure MTS within a limited time during FSE. In the future, it is necessary to investigate the relationships between each pathological tumor size in FSE processed by our inflation method and the prognosis of lung cancer. In previous studies about the correlation between pathological tumor size and prognosis, the preparation methods for the specimens were not well-described [14–16]. Recently, several articles reported that invasive tumor size is an independent prognostic factor, and it may be a better predictor of prognosis than overall tumor size in lepidic predominant tumors [17–19]. Borczuk et al. reported that an invasion size of 5 mm or more measured by straight measurement on paraffin-fixed sections was an independent factor for poor prognosis [7]. However, many questions still remain on how to define the invasive area of the tumor, and we should clarify whether we can treat a tumor invasive size obtained with FSE in the same measured values as a tumor size obtained without FSE.

Future studies are needed for comparing the contraction rate of the tissues of FSE samples with those of paraffin fixed samples. Moreover, it is necessary to modify the inflation procedure to prevent contraction of FSTS and PSTS, which lead to misleading results about migration stage.

Recently, the significance of FSE in thoracic oncology increased, and the endeavor to standardize the methodology in FSE, including the definition pathological tumor size, is indispensable.

5. Conclusion

FSE using our inflating technique diagnosed malignancy with 100% accuracy. Moreover, there was a strong correlation between CT tumor size and the size indicated by each pathological tumor measurement. This indicates that our inflating technique of the specimen for FSE is appropriate. However, FSTS and PSTS were significantly smaller than CT tumor size, which resulted in stage migration, and pathological tumor size was considerably underestimated for tumors classified as "air-containing type" tumors or "lepidic predominant" tumors that were measured based on PSTS. We propose that the pathological tumor size should be defined as the MTS in small lung adenocarcinomas in FSE.

Conflict of interest statement

None declared.

References

[1] Marchevsky AM, Changsri C, Gupta I, Fuller C, Houck W, McKenna Jr RJ. Frozen section diagnoses of small pulmonary nodules: accuracy and clinical implications. Ann Thorac Surg 2004;78:1755–9.

[2] Walts AE, Marchevsky AM. Root cause analysis of problems in the frozen section diagnosis of in situ, minimally invasive, and invasive adenocarcinoma of the lung. Arch Pathol Lab Med 2012;136:1515–21.

[3] Sirmali M, Demirağ F, Türüt H, Gezer S, Topçu S, Kaya S, et al. Utility of intraoperative frozen section examination in thoracic surgery. A review of 721 cases. Cardiovasc Surg (Torino) 2006;47:83–7.

[4] Novis DA, Zarbo RJ. Interinstitutional comparison of frozen section turnaround time. A College of American Pathologists Q-Probes study of 32868 frozen sections in 700 hospitals. Arch Pathol Lab Med 1997;121:559–67.

[5] Gephardt GN, Zarbo RJ. Interinstitutional comparison of frozen section consultations. A college of American pathologists Q-probes study of 90,538 cases in 461 institutions. Arch Pathol Lab Med 1996;120:804–9.

[6] Xu X, Chung JH, Jheon S, Sung SW, Lee CT, Lee JH, et al. The accuracy of frozen section diagnosis of pulmonary nodules: evaluation of inflation method during intraoperative pathology consultation with cryosection. J Thorac Oncol 2010;5:39–44.

[7] Borczuk AC, Qian F, Kazeros A, Eleazar J, Assaad A, Sonett JR, et al. Invasive size is an independent predictor of survival in pulmonary adenocarcinoma. Am J Surg Pathol 2009;33:462–9.

[8] Myung JK, Choe G, Chung DH, Seo JW, Jheon S, Lee CT, et al. A simple inflation method for frozen section diagnosis of minute precancerous lesions of the lung. Lung Cancer 2008;59:198–202.

[9] Travis WD, Brambilla E, Noguchi M, Nicholson AG, Geisinger K, Yatabe Y, et al. Diagnosis of lung adenocarcinoma in resected specimens: implications of the 2011 International Association for the Study of Lung Cancer/American Thoracic Society/European Respiratory Society classification. Arch Pathol Lab Med 2013;137:685–705.

[10] Kondo T, Yamada K, Noda K, Nakayama H, Kameda Y. Radiologic-prognostic correlation in patients with small pulmonary adenocarcinomas. Lung Cancer 2002;36:49–57.

[11] Saito H, Kameda Y, Masui K, Murakami S, Kondo T, Ito H, et al. Correlations between thin-section CT findings, histopathological and clinical findings of small pulmonary adenocarcinomas. Lung Cancer 2011;71:137–43.

[12] Borczuk AC. Assessment of invasion in lung adenocarcinoma classification, including adenocarcinoma in situ and minimally invasive adenocarcinoma. Mod Pathol 2012;25(Suppl. 1):S1–10.

[13] Lampen-Sachar K, Zhao B, Zheng J, Moskowitz CS, Schwartz LH, Zakowski MF, et al. Correlation between tumor measurement on Computed Tomography and resected specimen size in lung adenocarcinomas. Lung Cancer 2012;75:332–5.

[14] Ou SH, Zell JA, Ziogas A, Anton-Culver H. Prognostic factors for survival of stage I nonsmall cell lung cancer patients: a population-based analysis of 19,702 stage I patients in the California Cancer Registry from 1989 to 2003. Cancer 2007;110:1532–41.

[15] Port JL, Kent MS, Korst RJ, Libby D, Pasmantier M, Altorki NK. Tumor size predicts survival within stage IA non-small cell lung cancer. Chest 2003;124:1828–33.

[16] Tantraworasin A, Saeteng S, Lertprasertsuke N, Arreyakajohn N, Kasemsarn C, Patumanond J. Prognostic factors of tumor recurrence in completely resected non-small cell lung cancer. Cancer Manag Res 2013;5:77–84.

[17] Yoshizawa A, Motoi N, Riely GJ, Sima CS, Gerald WL, Kris MG, et al. Impact of proposed IASLC/ATS/ERS classification of lung adenocarcinoma: prognostic subgroups and implications for further revision of staging based on analysis of 514 stage I cases. Mod Pathol 2011;24:653–64.

[18] Warth A, Muley T, Meister M, Stenzinger A, Thomas M, Schirmacher P, et al. Back to the roots: the novel histologic IASLC/ATS/ERS classification system of invasive pulmonary adenocarcinoma is a stage-independent predictor of survival. J Clin Oncol 2012;30:1438–46.

[19] Tsutani Y, Miyata Y, Nakayama H, Okumura S, Adachi S, Yoshimura M, et al. Prognostic significance of using solid versus whole tumor size on high-resolution computed tomography for predicting pathologic malignant grade of tumors in clinical stage IA lung adenocarcinoma: a multicenter study. J Thorac Cardiovasc Surg 2011;143:607–12.

Lung Cancer 84 (2014) 254–258

Contents lists available at ScienceDirect

Lung Cancer

journal homepage: www.elsevier.com/locate/lungcan

A pilot study of adjuvant chemotherapy with irinotecan and cisplatin for completely resected high-grade pulmonary neuroendocrine carcinoma (large cell neuroendocrine carcinoma and small cell lung cancer)

Hirotsugu Kenmotsu[a,*], Seiji Niho[b], Takeo Ito[c], Yuichi Ishikawa[d], Masayuki Noguchi[e], Hirohito Tada[f], Ikuo Sekine[g], Shun-ichi Watanabe[h], Masahiro Yoshimura[i], Nobuyuki Yamamoto[a], Fumihiro Oshita[j], Kaoru Kubota[k], Kanji Nagai[l]

[a] Division of Thoracic Oncology, Shizuoka Cancer Center, Shizuoka, Japan
[b] Division of Thoracic Oncology, National Cancer Center Hospital East, Chiba, Japan
[c] Division of Pulmonary Medicine, Kuroki Memorial Hospital, Oita, Japan
[d] Division of Pathology, Cancer Institute, Japanese Foundation for Cancer Research, Tokyo, Japan
[e] Department of Pathology, Faculty of Medicine, University of Tsukuba, Ibaraki, Japan
[f] Department of General Thoracic Surgery, Osaka City General Hospital, Osaka, Japan
[g] Department of Medical Oncology, Graduate School of Medicine, Chiba University, Chiba, Japan
[h] Division of Thoracic Surgery, National Cancer Center Hospital, Tokyo, Japan
[i] Division of Thoracic Surgery, Hyogo Cancer Center, Hyogo, Japan
[j] Department of Thoracic Oncology, Kanagawa Cancer Center, Yokohama, Japan
[k] Medical Oncology Division, Nippon Medical School Hospital Cancer Center, Tokyo, Japan
[l] Division of Thoracic Surgery, National Cancer Center Hospital East, Chiba, Japan

ARTICLE INFO

Article history:
Received 24 October 2013
Received in revised form 18 January 2014
Accepted 4 March 2014

Keywords:
Lung cancer
High-grade neuroendocrine carcinoma
Small cell carcinoma
Large cell neuroendocrine carcinoma
Adjuvant chemotherapy

ABSTRACT

Background: Large cell neuroendocrine carcinoma (LCNEC) and small cell lung cancer (SCLC) are recognized as high-grade neuroendocrine carcinomas (HGNEC) of the lung. In patients with completely resected HGNEC, platinum-based adjuvant chemotherapy may be considered. However, the optimum chemotherapy regimen has not been determined. We conducted a multicenter single-arm phase II trial to evaluate irinotecan and cisplatin in postoperative adjuvant chemotherapy for HGNEC patients.

Patients and methods: Patients with completely resected stage I–IIIA HGNEC received four cycles of irinotecan (60 mg/m^2, day 1, 8, 15) plus cisplatin (60 mg/m^2, day 1). This regimen was repeated every 4 weeks. The primary endpoint was the rate of completion of chemotherapy (defined as having undergone three or four cycles), and secondary endpoints were the rate of 3-year relapse-free survival (RFS), rate of 3-year survival and toxicities.

Results: Forty patients were enrolled between September 2007 and April 2010. Patients' characteristics were: median age (range) 65 [45–73] years; male 85%; ECOG-PS 1 60%; LCNEC 57% and SCLC 43%; stage IA/IB/IIB/IIIA 32/35/8/5%; 95% received lobectomy. The rate of completion of chemotherapy was 83% (90% C.I.; 71–90%). The rate of overall survival at 3 years was estimated at 81%, and that of RFS at 3 years was 74%. The rates of overall survival and RFS at 3 years were 86 and 74% among 23 LCNEC patients, and 74 and 76% among 17 SCLC patients, respectively. Nineteen patients (48%) experienced grade 3 or 4 neutropenia, but only five patients (13%) developed febrile neutropenia. Two patients (5%) developed grade 3 diarrhea, and four patients (10%) had grade 3 nausea. No treatment-related deaths were observed in this study. All 40 specimens were also diagnosed as HGNEC by central pathological review.

Conclusions: The combination of irinotecan and cisplatin as postoperative adjuvant chemotherapy was feasible and possibly efficacious for resected HGNEC.

* Corresponding author at: Division of Thoracic Oncology, Shizuoka Cancer Center, 1007 Shimonagakubo, Nagaizumi-cho, Sunto-gun, Shizuoka 411-8777, Japan. Tel.: +81 55 989 5222; fax: +81 55 989 5634.
E-mail address: h.kenmotsu@scchr.jp (H. Kenmotsu).

http://dx.doi.org/10.1016/j.lungcan.2014.03.007
0169-5002/

1. Introduction

In 1991, Travis et al. proposed the classification of neuroendocrine tumor of the lung, including typical carcinoid, atypical carcinoid, large cell neuroendocrine carcinoma (LCNEC), and small cell carcinoma (SCLC) [1]. In addition, LCNEC and SCLC are recognized as high-grade neuroendocrine carcinomas (HGNEC) of the lung. LCNEC and SCLC share several histological features, including rosette formation, molding of nuclei, and lack of apparent glandular formation and keratinization [2,3].

LCNEC accounts for approximately 3% of all pulmonary malignancies, and SCLC accounts for 12%. In a large-scale, Japanese multi-institutional study of surgically resected pulmonary neuroendocrine tumors, there was no difference between LCNEC and SCLC in terms of overall survival. The survival curves were superimposed and the 5-year survival rates of surgically resected LCNEC and SCLC were 40.3 and 35.7%, respectively [4].

Retrospective analysis suggested that adjuvant chemotherapy using an SCLC-based standard regimen might be effective for LCNEC [5]. In patients with completely resected SCLC, platinum-based adjuvant chemotherapy may be considered [6,7]. The combination of cisplatin and etoposide as adjuvant chemotherapy is reported to be a feasible regimen and results in a favorable profile for SCLC [8]. However, the optimum chemotherapy regimen has not been determined. Combination chemotherapy with cisplatin and irinotecan is a standard treatment in Japan for extensive SCLC, and has been demonstrated to yield significantly longer overall survival than cisplatin and etoposide in the Japan Clinical Oncology Group Study 9511 [9]. Although LCNEC is now classified as non-small cell lung cancer (NSCLC) in WHO criteria, this combination has also been reported to be active for NSCLC [10]. Therefore, we conducted a multicenter phase II trial to evaluate irinotecan and cisplatin in postoperative adjuvant chemotherapy for completely resected HGNEC.

2. Patients and methods

2.1. Study design

This prospective phase II trial was conducted at 12 centers in Japan. It was approved by the institutional review boards of all participating centers, and all patients provided written informed consent. This study was registered at the UMIN Clinical Trial Registry (UMIN000001319).

2.2. Patients

Eligible patients were aged 20–74 years and histologically confirmed LCNEC and SCLC, completely resected, pathological stage IA, IB, IIA, IIB and IIIA. Patients were also required to have: the ability to start chemotherapy within 4–10 weeks after surgery; an Eastern Cooperative Oncology Group Performance Status (ECOG PS) of 0 or 1; no prior chemotherapy or radiotherapy; and adequate organ function (i.e., total bilirubin $\leq$1.5 mg/dL, aspartate aminotransferase (AST) and alanine aminotransferase (ALT) <100 IU/L, serum creatinine $\leq$1.5 mg/dL, leukocyte count $\geq$4000/mm^3, hemoglobin $\geq$9.5 g/dL, platelets $\geq$100,000/mm^3, and PaO_2 at room air $\geq$70 torr). Patients without UGT1A1 polymorphisms (homozygous for *6 or *28, simultaneously heterozygous *6 and *28), associated with irinotecan-related severe toxicity, were included. Key exclusion criteria were: interstitial pneumonia or pulmonary fibrosis; watery diarrhea; and intestinal obstruction or paralysis.

2.3. Treatment

Patients received 60 mg/m^2 of cisplatin on day 1 and 60 mg/m^2 of irinotecan on days 1, 8, and 15, every 4 weeks, up to four cycles if neither unacceptable toxicity nor recurrence was observed. The administration of irinotecan on day 8 or 15 was skipped if a leukocyte count <3000/mm^3, platelets <75,000/mm^3, symptoms of infection, diarrhea within 24 h, and/or grade 3 nonhematological toxicities developed. In the event of grade 4 leukopenia or thrombocytopenia, grade 2 or 3 diarrhea, or grade 3 nonhematological toxicities except nausea, vomiting, hyponatremia, and creatinine, the dose of irinotecan at the next cycle was reduced to 50 mg/m^2.

When the next cycle of chemotherapy was started, each patient was required to meet the following criteria: ECOG PS of 0 or 1, leukocyte count $\geq$3000/mm^3, platelets $\geq$100,000/mm^3, total bilirubin $\leq$1.5 mg/dL, AST and ALT <100 IU/L, serum creatinine $\leq$1.5 mg/dL, no symptoms of infection, and no diarrhea within 24 h.

Recurrence evaluations with CT scans for chest and abdomen have been performed every 6 months until 3 years. In addition, systemic evaluation, with CT scans for chest and abdomen; with CT or MRI for head; with bone scintigraphy or PET, has been performed at 3 years.

2.4. Pathological review

Surgically resected specimens including hematoxylin-eosin stained sections and immunohistochemistry of neuroendocrine markers, which were selected by institutional pathologists, were centrally reviewed by seven expert pathologists (T.K., M.N., K.T., Y.I., K.I., G.I., and J.S.-X.) blind to clinical information. The pathology panel members performed an independent pathology review, and the final diagnosis was established by mutual agreement.

2.5. Statistical analysis

The primary endpoint was rate of completion of chemotherapy, which was defined as the rate of patients who underwent the planned three or four cycles of irinotecan and cisplatin. Secondary endpoints included rate of 3-year relapse-free survival (RFS), rate of 3-year survival, and toxicities. Efficacy and safety analyses were performed on all patients who received at least one dose of the study treatment. Adverse events (AEs) were graded according to the National Cancer Institute Common Terminology Criteria for Adverse Events version 3.0.

In accordance with the minimax two-stage phase II study design by Simon, the treatment program was designed to refuse a completion rate of chemotherapy of 60% (P0) and to provide a significance level of .05 with a statistical power of 80% in assessing the feasibility of the regimen as an 80% completion rate (P1). The upper limit for first-stage drug rejection was eight completions in the 13 assessable patients; the upper limit of second-stage rejection was 25 completions within the cohort of 35 assessable patients.

Overall survival was defined as the interval between enrollment in this study and death or the final follow-up visit. The overall survival and RFS were estimated using the Kaplan–Meier analysis method.

3. Results

Forty patients were enrolled between September 2007 and April 2010, and all patients were eligible. The clinical data cut-off date was May 2013 for the analysis of efficacy, including overall survival and RFS.

Table 1
Patient characteristics (overall, $n = 40$).

	All	(%)	LCNEC	(%)	SCLC	(%)
Number of patients	40		23		17	
Gender						
Male	34	(85)	20	(87)	14	(82)
Female	6	(15)	3	(13)	3	(18)
Age, year						
Median	65		61		67	
(range)	(45–73)		(45–71)		(50–73)	
Performance status (ECOG)						
0	16	(40)	8	(35)	8	(47)
1	24	(60)	15	(65)	9	(53)
Surgical procedure						
Lobectomy	38	(95)	22	(96)	16	(94)
Pneumonectomy	1	(3)	1	(4)		
Segmentectomy	1	(3)			1	(6)
Pathological stage						
IA	13	(32)	3	(13)	10	(59)
IB	14	(35)	11	(48)	3	(18)
IIA	0		0		0	
IIB	7	(18)	6	(26)	1	(5)
IIIA	6	(15)	3	(13)	3	(18)

SCLC: Small cell lung carcinoma, LCNEC: Large cell neuroendocrine carcinoma.

Table 2
Treatment delivery of adjuvant chemotherapy.

Number of cycles	Number of patients	(%)
1	6	15
2	1	3
3	2	5
4	31	77

3.1. Patient characteristics

Table 1 summarizes the baseline characteristics of the 40 patients enrolled in this study. The median age was 65 years, and 85% of the patients were male. Histologically, SCLC and LCNEC were observed in 43 and 57%, respectively. Sixty-seven percent of the patients were diagnosed as pathological stage I. Forty-eight percent of LCNEC patients were diagnosed as pathological stage IB, and 59% of SCLC patients as pathological stage IA.

3.2. Treatment compliance

Thirty-three patients underwent the planned three or four cycles of planned adjuvant chemotherapy (Table 2). The rate of completion of chemotherapy was 83% (90% confidence interval (CI); 71–90%). However, seven patients received one or two cycles, because of adverse events in three patients (grade 3 diarrhea, cerebral hemorrhage, grade 2 enuresis) and treatment refusal in four patients. Nine patients experienced dose reduction, and 21 patients skipped administration of irinotecan. The dose intensity (the actual dose delivered as a proportion of the planned dose) was 74% for irinotecan and 87% for cisplatin.

3.3. Overall survival and recurrence-free survival

Overall survival and RFS data are shown in Fig. 1, with median follow-up for overall survival of 49 months. The rate of overall survival at 3 years was estimated at 81% (95% CI; 69–95%), and that of RFS at 3 years was 74% (95% CI; 61–90%). The rates of overall survival and RFS at 3 years were 86 and 74% among 23 LCNEC patients, and 74 and 76% among 17 SCLC patients, respectively (Fig. 2).

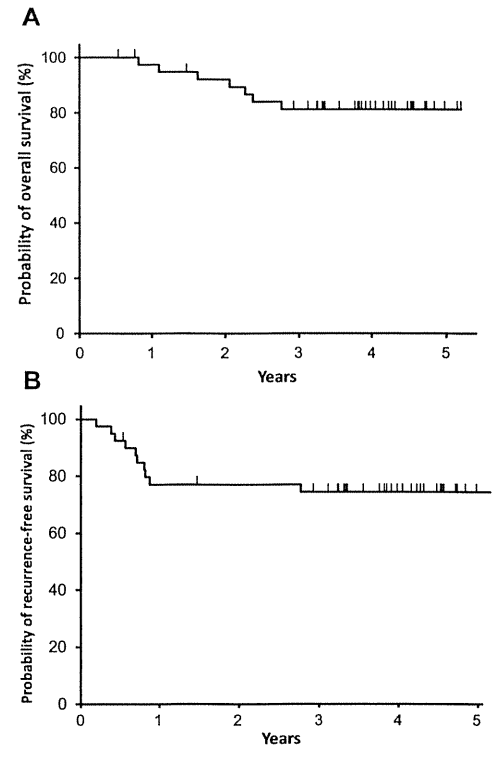

Fig. 1. (A) Overall survival curve including all eligible 40 patients. (B) Recurrence-free survival curve including all eligible 40 patients.

3.4. Safety and adverse events

Table 3 shows the incidence of AEs evaluated in all eligible patients. The most common toxicity was neutropenia. Nineteen patients (48%) experienced grade 3 or 4 neutropenia, but only five patients (13%) developed febrile neutropenia. Two patients (5%) developed grade 3 diarrhea, and four patients (10%) had grade 3 nausea. There were no treatment-related deaths in this trial.

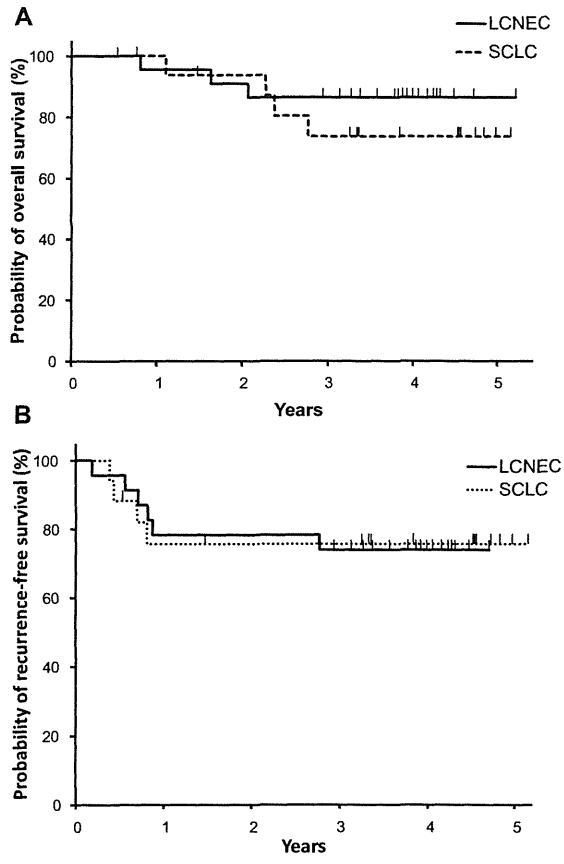

Fig. 2. (A) Overall survival curve for 23 large cell neuroendocrine carcinoma (LCNEC) patients and 17 SCLC patients. (B) Recurrence-free survival curve for 23 LCNEC patients and 17 small cell lung cancer (SCLC) patients.

3.5. Central pathological diagnosis

Pathological specimens for central review were available in all 40 patients. Twenty-eight specimens showed complete concordance of central pathological diagnosis among the seven expert pathologists. All 40 specimens were diagnosed as HGNEC at the central pathological review. There were two specimens that showed a difference between the institutional diagnosis and central pathological diagnosis. These specimens were diagnosed as LCNEC at each institution, and diagnosed as SCLC at the central pathological review.

Table 3
Treatment-related adverse events (overall, $n = 40$).

Toxicity	toxicity grade			%3–4
	2	3	4	
Leukocytes	18	7	0	18
Neutrophils	12	15	4	48
Hemoglobin	15	6	4	25
Platelets	2	0	0	0
Febrile neutropenia	–	5	0	13
Bilirubin	0	0	0	0
AST	0	0	0	0
ALT	1	0	0	0
Creatinine	0	0	0	0
Hyponatremia	0	6	0	15
Hypokalemia	0	4	0	10
Hyperkalemia	3	1	0	3
Nausea	8	4	–	10
Vomiting	4	2	0	5
Anorexia	12	4	0	10
Diarrhea	11	2	0	5
Fatigue	10	5	0	13
Constipation	3	0	0	0
Alopecia	7	–	–	0
Infection	2	0	0	0

AST: Aspartate transaminase, ALT: Alanine transaminase.

4. Discussion

Irinotecan and cisplatin showed acceptable toxicities and favorable feasibility as postoperative adjuvant chemotherapy for HGNEC of the lung. This study is the first prospective trial to evaluate the postoperative adjuvant chemotherapy of irinotecan and cisplatin for HGNEC. Although there have been no reports on a randomized trial of postoperative adjuvant chemotherapy for HGNEC, previous reports suggest the efficacy of postoperative adjuvant chemotherapy for very limited SCLC compared with surgery alone [11–15]. In addition, the guidelines of the European Society for Medical Oncology (ESMO) and American College of Chest Physicians (ACCP) recommend postoperative adjuvant chemotherapy for resected SCLC [7,16]. To our knowledge, there have been few prospective trials on postoperative adjuvant chemotherapy for resected SCLC [8,17], and only one trial for resected LCNEC [18]. In a phase II trial of adjuvant cisplatin and etoposide for resected SCLC, the 3-year survival rate was 61% [8]. In this study, the rate of overall survival at 3 years was estimated at 81%, and that of RFS at 3 years was 77%. Therefore, the combination of irinotecan and cisplatin could be effective.

The combination of irinotecan and cisplatin has been reported to be effective for extensive SCLC [9,19–21]. Retrospective analyses demonstrated that patients with advanced LCNEC who were treated with SCLC regimens, including irinotecan and cisplatin, had a better response rate and OS than those who were treated with non-small cell lung cancer (NSCLC) regimens [5,22–24]. Also, in the adjuvant setting, SCLC regimens are reported to be effective [5]. We conducted a phase II study of combination chemotherapy with irinotecan and cisplatin in 44 patients with advanced LCNEC, and the response rate and progression-free survival were 54.5% and 5.9 months, respectively [25].

In a phase II trial of adjuvant cisplatin and etoposide for resected SCLC, 77% of the patients underwent the planned three or four cycles of adjuvant chemotherapy [8]. Compliance of adjuvant chemotherapy for resected NSCLC showed that 48–74% of the patients completed the planned cycles [26–28]. In this study, 33 patients (83%) underwent the planned three or four cycles of adjuvant chemotherapy, and this compliance is comparable to these studies. The most common toxicity in our study was grade 3 or 4 neutropenia (48%), and grade 3 diarrhea was observed in only 5% of the patients. Toxicities were similar to previous reports of irinotecan and cisplatin in extensive SCLC [9,29]. Combination chemotherapy of irinotecan and cisplatin as adjuvant chemotherapy was safe with good compliance.

In conclusion, the combination chemotherapy of irinotecan and cisplatin as postoperative adjuvant chemotherapy was feasible and active in patients with resected HGNEC. This is the first prospective study of postoperative adjuvant chemotherapy for resected HGNEC. In Japan, a randomized phase III trial is ongoing to evaluate adjuvant chemotherapy of irinotecan and cisplatin, compared with etoposide and cisplatin, for completely resected HGNEC (Japan Clinical Oncology Group 1205/1206).

Funding

This work was supported in part by a National Cancer Center Research and Development Fund (23-A-18), a Grant-in-Aid for

Cancer Research (17S-2) from the Ministry of Health, Labour and Welfare and a Grant from the Ministry of Health, Labour and Welfare for the Third-Term Comprehensive Strategy for Cancer Control, Japan.

Conflict of interest statement

The authors indicate no potential conflicts of interest.

Acknowledgments

We thank all the patients who participated in this study and their families. We also thank Ms. Fumiko Koh, Ms. Eriko Imai and Ms. Reiko Kashiwabara for data management, Dr. Toru Kameya (Shizuoka Cancer Center, Shizuoka), Dr. Koji Tsuta (National Cancer Center Hospital, Tokyo), Dr. Genichiro Ishii (National Cancer Center Hospital East, Chiba), Dr. Ken Inoue (Osaka City General Hospital, Osaka), and Dr. Shi-Xu Jaing (Kitasato University, Kanagawa) for central pathological review, and Dr. Makoto Nishio (Cancer Institute Hospital, Japanese Foundation for Cancer Research, Tokyo), Dr. Naoyuki Nogami (NHO Shikoku Cancer Center, Matsuyama), Dr. Rie Nakahara (Tochigi Cancer Center, Utsunomiya), Dr. Hideshi Takei (Kyorin University School of Medicine, Tokyo), Dr. Norihiko Ikeda (Tokyo Medical University, Tokyo), Dr. Toyoaki Hida (Aichi Cancer Center Hospital, Aichi), Dr. Satoh Yukitoshi (Kitasato University, Kanagawa), and Mr. Keita Mori (Biostatistician, Shizuoka Cancer Center) for their contributions to this study.

References

[1] Travis WD, Linnoila RI, Tsokos MG, Hitchcock CL, Cutler Jr GB, Nieman L, et al. Neuroendocrine tumors of the lung with proposed criteria for large-cell neuroendocrine carcinoma. An ultrastructural, immunohistochemical, and flow cytometric study of 35 cases. Am J Surg Pathol 1991;15(June (6)):529–53.
[2] Cerilli LA, Ritter JH, Mills SE, Wick MR. Neuroendocrine neoplasms of the lung. Am J Clin Pathol 2001;116(December (Suppl.)):S65–96.
[3] Marchevsky AM, Gal AA, Shah S, Koss MN. Morphometry confirms the presence of considerable nuclear size overlap between small cells and large cells in high-grade pulmonary neuroendocrine neoplasms. Am J Clin Pathol 2001;116(October (4)):466–72.
[4] Asamura H, Kameya T, Matsuno Y, Noguchi M, Tada H, Ishikawa Y, et al. Neuroendocrine neoplasms of the lung: a prognostic spectrum. J Clin Oncol 2006;24(January (1)):70–6.
[5] Rossi G, Cavazza A, Marchioni A, Longo L, Migaldi M, Sartori G, et al. Role of chemotherapy and the receptor tyrosine kinases KIT, PDGFRalpha PDGFRbeta, and Met in large-cell neuroendocrine carcinoma of the lung. J Clin Oncol 2005;23(December (34)):8774–85.
[6] Sorensen M, Pijls-Johannesma M, Felip E. Small-cell lung cancer: ESMO Clinical Practice Guidelines for diagnosis, treatment and follow-up. Ann Oncol 2010;21(May (Suppl. 5)):v120–5.
[7] Simon GR, Turrisi A. Management of small cell lung cancer: ACCP evidence-based clinical practice guidelines (2nd edition). Chest 2007;132(September (3 Suppl.)):324S–39S.
[8] Tsuchiya R, Suzuki K, Ichinose Y, Watanabe Y, Yaumitsu T, Ishizuka N, et al. Phase II trial of postoperative adjuvant cisplatin and etoposide in patients with completely resected stage I–IIIa small cell lung cancer: the Japan Clinical Oncology Lung Cancer StudyGroup Trial (JCOG9101). J Thorac Cardiovasc Surg 2005;129(May (5)):977–83.
[9] Noda K, Nishiwaki Y, Kawahara M, Negoro S, Sugiura T, Yokoyama A, et al. Irinotecan plus cisplatin compared with etoposide plus cisplatin for extensive small-cell lung cancer. N Engl J Med 2002;346(January (2)):85–91.
[10] Ohe Y, Ohashi Y, Kubota K, Tamura T, Nakagawa K, Negoro S, et al. Randomized phase III study of cisplatin plus irinotecan versus carboplatin plus paclitaxel, cisplatin plus gemcitabine, and cisplatin plus vinorelbine for advanced non-small-cell lung cancer: Four-Arm Cooperative Study in Japan. Ann Oncol 2007;18(February (2)):317–23.
[11] Shore DF, Paneth M. Survival after resection of small cell carcinoma of the bronchus. Thorax 1980;35(November (11)):819–22.
[12] Sorensen HR, Lund C, Alstrup P. Survival in small cell lung carcinoma after surgery. Thorax 1986;41(June (6)):479–82.
[13] Prasad US, Naylor AR, Walker WS, Lamb D, Cameron EW, Walbaum PR. Long term survival after pulmonary resection for small cell carcinoma of the lung. Thorax 1989;44(October (10)):784–7.
[14] Shah SS, Thompson J, Goldstraw P. Results of operation without adjuvant therapy in the treatment of small cell lung cancer. Ann Thorac Surg 1992;54(September (3)):498–501.
[15] Coolen L, Van den Eeckhout A, Deneffe G, Demedts M, Vansteenkiste J. Surgical treatment of small cell lung cancer. Eur J Cardiothorac Surg 1995;9(2):59–64.
[16] Stahel R, Thatcher N, Fruh M, Le Pechoux C, Postmus PE, Sorensen JB, et al. 1st ESMO consensus conference in lung cancer; Lugano 2010: small-cell lung cancer. Ann Oncol 2011;22(September (9)):1973–80.
[17] Davis S, Crino L, Tonato M, Darwish S, Pelicci PG, Grignani F. A prospective analysis of chemotherapy following surgical resection of clinical stage I–II small-cell lung cancer. Am J Clin Oncol 1993;16(April (2)):93–5.
[18] Iyoda A, Hiroshima K, Moriya Y, Takiguchi Y, Sekine Y, Shibuya K, et al. Prospective study of adjuvant chemotherapy for pulmonary large cell neuroendocrine carcinoma. Ann Thorac Surg 2006;82(November (5)):1802–7.
[19] Lara Jr PN, Natale R, Crowley J, Lenz HJ, Redman MW, Carleton JE, et al. Phase III trial of irinotecan/cisplatin compared with etoposide/cisplatin in extensive-stage small-cell lung cancer: clinical and pharmacogenomic results from SWOG S0124. J Clin Oncol 2009;27(May (15)):2530–5.
[20] Hanna N, Bunn Jr PA, Langer C, Einhorn L, Guthrie Jr T, Beck T, et al. Randomized phase III trial comparing irinotecan/cisplatin with etoposide/cisplatin in patients with previously untreated extensive-stage disease small-cell lung cancer. J Clin Oncol 2006 May 1;24(13):2038–43.
[21] Jiang J, Liang X, Zhou X, Huang L, Huanz R, Chu Z, et al. A meta-analysis of randomized controlled trials comparing irinotecan/platinum with etoposide/platinum in patients with previously untreated extensive-stage small cell lung cancer. J Thorac Oncol 2010;5(June (6)):867–73.
[22] Sun JM, Ahn MJ, Ahn JS, Um SW, Kim H, Kim HK, et al. Chemotherapy for pulmonary large cell neuroendocrine carcinoma: similar to that for small cell lung cancer or non-small cell lung cancer? Lung Cancer 2012;77(August (2)):365–70.
[23] Fujiwara Y, Sekine I, Tsuta K, Ohe Y, Kunitoh H, Yamamoto N, et al. Effect of platinum combined with irinotecan or paclitaxel against large cell neuroendocrine carcinoma of the lung. Jpn J Clin Oncol 2007;37(July (7)):482–6.
[24] Igawa S, Watanabe R, Ito I, Murakami H, Takahashi T, Nakamura Y, et al. Comparison of chemotherapy for unresectable pulmonary high-grade non-small cell neuroendocrine carcinoma and small-cell lung cancer. Lung Cancer 2010;68(June (3)):438–45.
[25] Niho S, Kenmotsu H, Sekine I, Ishii G, Ishikawa Y, Noguchi M, et al. Combination chemotherapy with irinotecan and cisplatin for large-cell neuroendocrine carcinoma of the lung: a multicenter phase II study. J Thorac Oncol 2013;8(July (7)):980–4.
[26] Winton T, Livingston R, Johnson D, Rigas J, Johnston M, Butts C, et al. Vinorelbine plus cisplatin vs. observation in resected non-small-cell lung cancer. N Engl J Med 2005;352(June (25)):2589–97.
[27] Arriagada R, Bergman B, Dunant A, Le Chevalier T, Pignon JP, Vansteenkiste J. Cisplatin-based adjuvant chemotherapy in patients with completely resected non-small-cell lung cancer. N Engl J Med 2004;350(January (4)): 351–60.
[28] Douillard JY, Rosell R, De Lena M, Carpagnano F, Ramlau R, Gonzales-Larriba JL, et al. Adjuvant vinorelbine plus cisplatin versus observation in patients with completely resected stage IB–IIIA non-small-cell lung cancer (Adjuvant Navelbine International Trialist Association [ANITA]): a randomised controlled trial. Lancet Oncol 2006;7(September (9)):719–27.
[29] Natale RB, Lara PN, Chansky K, Crowley JJ, Jett JR, Carleton JE, et al. S0124: a randomized phase III trial comparing irinotecan/cisplatin (IP) with etoposide/cisplatin (EP) in patients (pts) with previously untreated extensive stage small cell lung cancer (E-SCLC). ASCO Meeting Abstract. J Clin Oncol 2008;26(May (Suppl. 15)):7512.

Cancer Medicine

Open Access

ORIGINAL RESEARCH

Long noncoding RNA *HOTAIR* is relevant to cellular proliferation, invasiveness, and clinical relapse in small-cell lung cancer

Hiroshi Ono[1,2], Noriko Motoi[1], Hiroko Nagano[1], Eisaku Miyauchi[1], Masaru Ushijima[3], Masaaki Matsuura[3,4], Sakae Okumura[5], Makoto Nishio[5], Tetsuro Hirose[6], Naohiko Inase[2] & Yuichi Ishikawa[1]

[1]Division of Pathology, The Cancer Institute, Japanese Foundation for Cancer Research, Tokyo, Japan
[2]Department of Integrated Pulmonology, Tokyo Medical and Dental University, Tokyo, Japan
[3]Bioinformatics Group, Genome Center, Japanese Foundation for Cancer Research, Tokyo, Japan
[4]Division of Cancer Genomics, The Cancer Institute, Japanese Foundation for Cancer Research, Tokyo, Japan
[5]Thoracic Oncology Center, The Cancer Institute Hospital, Japanese Foundation for Cancer Research, Tokyo, Japan
[6]Institute for Genetic Medicine, Hokkaido University, Sapporo, Japan

Keywords
HOTAIR, invasiveness, lincRNA, proliferation, small-cell lung cancer

Correspondence
Yuichi Ishikawa, Division of Pathology, The Cancer Institute, Japanese Foundation for Cancer Research, 3-8-31 Ariake, Koto-ku, Tokyo 135-8550, Japan.
Tel: +81-3-3570-0488; Fax: +81-3-3570-0558; E-mail: ishikawa@jfcr.or.jp

Funding Information
Parts of this study were supported financially by Grants-in-Aid for Scientific Research from the Ministry of Education, Culture, Sports, Science and Technology, Japan, grants from the Japan Society for the Promotion of Science, the Ministry of Health, Labour and Welfare, and the Princess Takamatsu Cancer Research Fund.

Received: 20 November 2013; Revised: 5 January 2014; Accepted: 23 January 2014

***Cancer Medicine* 2014; 3(3): 632–642**

doi: 10.1002/cam4.220

Abstract

Small-cell lung cancer (SCLC) is a subtype of lung cancer with poor prognosis. To identify accurate predictive biomarkers and effective therapeutic modalities, we focus on a long noncoding RNA, *Hox* transcript antisense intergenic RNA (*HOTAIR*), and investigated its expression, cellular functions, and clinical relevance in SCLC. In this study, *HOTAIR* expression was assessed in 35 surgical SCLC samples and 10 SCLC cell lines. The efficacy of knockdown of *HOTAIR* by siRNA transfection was evaluated in SBC-3 cells in vitro, and the gene expression was analyzed using microarray. *HOTAIR* was expressed highly in pure, rather than combined, SCLC ($P = 0.012$), that the subgroup with high expression had significantly more pure SCLC ($P = 0.04$), more lymphatic invasion ($P = 0.03$) and more relapse ($P = 0.04$) than the low-expression subgroup. The knockdown of *HOTAIR* in SBC-3 cells led to decreased proliferation activity and decreased invasiveness in vitro. Gene expression analysis indicated that depletion of *HOTAIR* resulted in upregulation of cell adhesion-related genes such as *ASTN1*, *PCDHA1*, and mucin production-related genes such as *MUC5AC*, and downregulation of genes involved in neuronal growth and signal transduction including *NTM* and *PTK2B*. Our results suggest that *HOTAIR* has an oncogenic role in SCLC and could be a prognostic biomarker and therapeutic target.

Introduction

Lung cancer is a leading cause of cancer death worldwide [1]. Small-cell lung cancer (SCLC) is an aggressive subtype, characterized by a neuroendocrine nature, which represents ~15% of all newly diagnosed lung cancers [2]. SCLC patients have a poor prognosis compared with non–small-cell lung cancers (NSCLCs) due to more rapid growth and more frequent recurrence. Although the survival of NSCLC patients has been significantly improved by targeted chemotherapy, there are currently no targeted drugs effective against SCLC. To identify accurate predictive biomarkers and to develop effective therapeutic modalities, elucidation

of molecular mechanisms underlying the rapid growth and the high propensity for relapse of SCLC is essential.

Advances in experimental technology have been applied to studies of malignant tumors including SCLC [3]. In particular, application of modern genetic profiling technology to the study of noncoding RNAs has revealed a crucial role for these molecules in tumor cell regulation. Similar to short regulatory noncoding RNAs (ncRNAs), such as microRNAs, many long intergenic ncRNAs (lincRNAs) have been found to be important by functioning as the interface between DNA and specific chromatin remodeling activities [3–7]. These lincRNAs are involved in diverse cellular processes, including cell-cycle regulation, immune surveillance, and stem cell pluripotency.

Hox transcript antisense intergenic RNA (*HOTAIR*) is one of the few biologically well-studied lincRNAs [8, 9]. Previous studies have demonstrated that *HOTAIR* is transcribed from *HoxC* gene as an antisense transcript, and binds polycomb repressive complex 2 (PRC2) and LSD1-CoREST-REST complex as scaffolds, leading to catalyzing trimethylation of H3K27 and spontaneous demethylation of H3K4, and to repressing transcription of *HoxD* genes [9]. REST (RE1 silencing transcriptional factor, also called neuron-restrictive silencer factor) and its corepressors negatively regulate neurogenesis and contribute to the maintenance of pluripotency of neural cells [10], whereas LSD1 (lysin-specific demethylase 1) regulates neural stem cell proliferation [11]. In relation to DNA methylation, EZH2, a compartment of PRC2, directly interacts with DNA methyltransferases (DNMT1, DNMT3A and DNMT3B). This interaction is necessary for maintenance of DNA methylation and stable repression of specific genes, including many tumor suppressors [12]. In fact, 20% of the lincRNAs have been shown to associate with PRC2. The homeobox-containing genes as targets of *HOTAIR* are a family of transcriptional regulators encoding DNA-binding homeodomains involved in the control of normal development [4, 5]. Also, aberrant expression of homeobox genes is associated with both morphological abnormalities and carcinogenesis [6, 7]. Moreover, a most recent study suggested that the role of *HOTAIR* in tumorigenesis occurs through triggering epithelial-to-mesenchymal transition (EMT) and acquiring stemness and its maintenance [13].

Although *HOTAIR* and its association in cancer metastasis and prognosis of diverse cancers have been suggested in several studies [14–22], its functions in SCLC remain unclear. In this study, we investigated the role of *HOTAIR* for cellular proliferation and patients' prognosis to develop a biomarker and a new target for therapy of SCLC.

Materials and Methods

Clinical samples and cell lines

Between January 1995 and December 2010, 3460 patients with primary lung cancer underwent surgery at the Cancer Institute Hospital of Japanese Foundation for Cancer Research (JFCR), Tokyo, Japan. Since SCLC is usually inoperable, only 55 (1.6%) cases had been diagnosed as SCLC by expert pathologists using hematoxylin and eosin (H&E) staining, based on the WHO classification [23].

Due to inadequate amounts of viable cancer cells, 20 cases were excluded from the study leaving 35 cases. Basis on TNM classification of malignant tumors 7th edition, all cases were staged. Specimens were snap-frozen in liquid nitrogen typically within 15 min after removal and stored at −80°C. Written informed consent for research was obtained from all patients, and our institutional review board approved the study plan. We collected clinicopathological details including neoadjuvant and adjuvant chemotherapy (NAC and AC, respectively), and listed them in Table 1.

Ten SCLC cell lines (COLO-668, COR-L51, COR-L88, DMS-79, DMS-53, Lu-134A, MS-1, SBC-3, SBC-5, and SBC-1), one adenocarcinoma cell line (A549) and a normal lung cell line (MRC-5), derived from embryonic normal lung tissue, were used. The former four lines were obtained from the European Collection of Cell Cultures, and the other were from Japanese Collection of Research Bio-resources or the RIKEN Bio Resource Center. All cells were maintained in the Dulbecco's modified Eagle's medium (DMEM) supplemented with 2 mmol/L L-alanyl-L-glutamine solution, 1.1% antibiotic-antimycotic mixed stock solution (Nacalai Tesque, Kyoto, Japan) and 10% fetal bovine serum (FBS), at 37°C, 5% CO_2 incubator.

Primary-cultured normal bronchial epithelial (NBE) cells were obtained from fresh surgical materials. Emergence and proliferation of bronchial epithelial cells around the samples without any proliferation of fibroblasts and contamination was confirmed by microscopy.

RNA preparation, reverse transcription, and quantitative real-time polymerase chain reaction

Total RNA from tissues and cells were extracted using the RNeasy mini kit or RNeasy mini kit plus (Qiagen, Tokyo, Japan). cDNAs were generated from 30 ng of total RNA. The resulting cDNA was subjected to a 45-cycle polymerase chain reaction (PCR) amplification step followed by quantitative real-time PCR (qRT-PCR) using

Table 1. Comparisons of clinicopathological factors of all SCLC patients enrolled (n = 35) and those with high- and low expression of *HOTAIR*.

	All cases, examined (n = 35)		Cases with high-*HOTAIR* expression (n = 12)		Cases with low-*HOTAIR* expression (n = 23)		
Factors	*N*	%	*N*	%	*N*	%	*P* value
Age (mean ± SD)	65.8 ± 6.60		63.3 ± 6.70		67.1 ± 6.30		0.10
Gender							
M	25	71.4	9	75.0	16	69.6	0.53
F	10	28.6	3	25.0	7	30.4	
Cumulative smoking (pack-years)	52 ± 31		52 ± 19		52 ± 36		0.96
Chemotherapy type							
NAC − AC−	3	8.60	1	8.33	2	8.70	
NAC + AC−	3	8.60	0	0	3	13.0	
NAC − AC+	23	65.7	8	66.7	15	65.2	
NAC + AC+	6	17.1	3	25.0	3	13.0	
Regimen							
NAC(n = 9)	CDDP + VP16 (8)	22.9	3	25.0	5	21.7	
	CDDP + DOC (1)	2.90	0	0	1	4.35	
AC(n = 29)	CDDP + VP16[1] (22)	62.9	10	83.3	12	52.2	
	CBDCA + VP16[2] (4)	11.4	0	0	4	17.4	
	Mix; 1 and 2 (3)	8.60	1	8.33	2	8.70	
Histological type (SCLC)							
Pure	24	68.6	11	91.7	13	56.5	0.04*
Combined	11	31.4	1	8.33	10	43.5	
	With Ad (5)	45.5	0	0	5	50.0	
	With LCC (2)	18.2	0	0	2	20.0	
	With LCNEC (4*)	36.4	1*	100	2	20.0	
	With others (1)	9.10	0	0	1	10.0	
	*include combined case (with both LCNEC/Ad)		*include combined case (with both LCNEC/Ad)				
Operation (SCLC)							
Partial resection	3	8.60	1	8.33	2	8.70	
Segmentectomy	0	0	0	0	0	0	
Lobectomy (1 lobe)	27	77.1	10	83.3	17	73.9	
Lobectomy + partial resection	1	2.90	1	8.33	0	0	
Lobectomy (2 lobes)	2	5.70	0	0	2	8.70	
Pneumectomy	2	5.70	0	0	2	8.70	
Pathological stage							
1a	11	31.4	1	8.33	10	43.5	
1b	4	11.4	2	16.7	2	8.70	
2a	7	20.0	3	25.0	4	17.4	
2b	2	5.70	0	0	2	8.70	
3a	10	28.6	6	50.0	4	17.4	
3b	1	2.90	0	0	1	4.35	
4	0	0	0	0	0	0	
Invasion (microscopic)							
Vascular invasion	29	82.9	9	75.0	20	87.0	0.33
Lymphatic invasion	20	57.1	10	83.3	10	43.5	0.03*
Relapse	15	42.9	8	66.7	7	30.4	0.04*
	Brain (6)	40.0	4	50.0	2	28.6	
	Lung (2)	13.3	2	25.0	0	0	
	Mediastinal LNs (4)	26.7	3	37.5	1	14.3	

Table 1. Continued.

Factors	All cases, examined (n = 35)		Cases with high-*HOTAIR* expression (n = 12)		Cases with low-*HOTAIR* expression (n = 23)		P value
	N	%	*N*	%	*N*	%	
	Stomach (1)	6.70	0	0	1	14.3	
	Liver (3)	20.0	1	12.5	2	28.6	
	Adrenal gl. (2)	5.70	1	12.5	1	14.3	
	Others (pleural eff.) (1)	6.70	0	0	1	14.3	
Survival							
Alive	19	54.3	5	41.7	14	60.9	
Dead	16	45.7	7	58.3	9	39.1	
	Lung cancer (11)	68.7	6	85.7	5	55.6	
	Other malignancy (2)	12.5	1	14.3	1	11.1	
	Other disease (2)	12.5	0	0	2	22.2	
	Unknown (1)	6.30	0	0	1	11.1	
DSS (mean ± SD)	45.3 ± 35.7 mos.		38.1 ± 27.2 mos		49.0 ± 39.5 mos		
RFS/DFS (SCLC) (mean ± SD)	40.9 ± 38.5 mos.		30.8 ± 30.7 mos		46.3 ± 41.6 mos		

SCLC, small-cell lung cancer; smoking index, a product of number of cigarettes per day by duration in years; NAC, neoadjuvant chemotherapy; AC, adjuvant chemotherapy; CDDP, cisplatin; CBDCA, carboplatin; VP-16, etoposide; DOC, docetaxel; Ad, adenocarcinoma; LCC, large cell carcinoma; LCNEC, large cell neuroendocrine carcinoma; LNs, lymph nodes; DSS, disease-specific survival; RFS, relapse-free survival; DFS, disease-free survival.
*$P < 0.05$.

the LightCycler 480 SYBR Green I Master protocol (Roche Applied Science, Indianapolis, IN). Triplicates were run for each gene for each sample as previously [16]. Based on previous studies [24], the amount of *HOTAIR* RNA was normalized to that of beta-actin (*ACTB*) in tissue samples and xenografts, and to Glyceraldehydes-3-phosphate dehydrogenase (*GAPDH*) in cell lines and normal cells. The *HOTAIR/ACTB* ratio in 35 SCLC and 15 noncancerous lung tissues randomly chosen from the 35 patients were analyzed by qRT-PCR. Tumors were divided into two groups with high- and low expression based on *HOTAIR/ACTB* ratios, using receiver operating characteristic (ROC) curve analysis. The primer sequences are listed in Table S1.

HOTAIR expression of SCLC cell lines as well as control cells

We assessed *HOTAIR* expression in above cell lines and normal controls, normalizing to *GAPDH*. To define high- and low-expression groups, we used the level of normal controls, that is, the cut-off level of high expression was defined as above those of normal controls.

SCLC cell xenografts

We examined *HOTAIR* expression in xenografts as well [25]. Four-week-old male nude mice *Crlj:CD1-Foxn1*^{NU} with ICR background were purchased from Charles River Laboratories, Japan, housed at the animal care facility of our institute and kept under standard temperature, humidity, and timed-lighting conditions and provided mouse chow and water ad libitum. The five SCLC cell lines with high expression (final concentration, 1.0×10^7 cells/0.3 mL phosphate buffered saline [PBS] each) were injected directly into three sites of the abdominal subcutaneous adipose tissue of the mice in 0.3 mL of sterile PBS. Developed tumors were immediately frozen in liquid nitrogen and stored at −80°C until use.

RNA interference

Cells were transfected with 20 nmol/L small interfering (si)RNAs targeting *HOTAIR*, using Lipofectamine RNAiMAX (Invitrogen, Carlsbad, CA) as per manufacturer's directions. Transfection efficiency was assessed using a fluorescence microscope (Leica-DMIRE2) following 72 h incubation after transfection of labeled positive control; BLOCK-iT Alexa Fluor Red Fluorescent Oligo (Invitrogen) according to manufacturer's procedures. Twenty nmol/L (final concentration) of siRNAs and 1.5 μL of Lipofectamine RNAiMAX in a total volume of 101.5 μL were used for transfection of SBC-3 cells in 24-well based analysis (transduction efficiency: 100%, knockdown efficiency: 50%). We transfected #1–3 si*HOTAIR* as previously [8, 9, 14] to SBC-3 cells. After 72 h, total RNAs were collected for qRT-PCR analysis. Primer sequences are listed in Table S1.